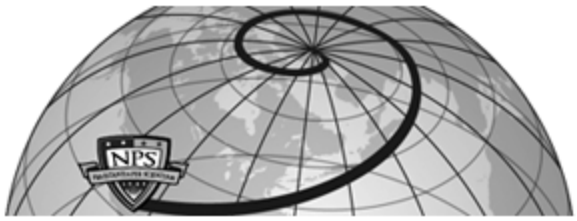

NAVAL POSTGRADUATE SCHOOL

MONTEREY, CALIFORNIA

THESIS

DISTURBANCE DETECTION IN SNOW USING POLARIMETRIC IMAGERY OF THE VISIBLE SPECTRUM

by

David C. West

December 2010

Thesis Advisor:	Richard C. Olsen
Second Reader:	David Trask

Approved for public release; distribution is unlimited

THIS PAGE INTENTIONALLY LEFT BLANK

REPORT DOCUMENTATION PAGE			Form Approved OMB No. 0704-0188
Public reporting burden for this collection of information is estimated to average 1 hour per response, including the time for reviewing instruction, searching existing data sources, gathering and maintaining the data needed, and completing and reviewing the collection of information. Send comments regarding this burden estimate or any other aspect of this collection of information, including suggestions for reducing this burden, to Washington headquarters Services, Directorate for Information Operations and Reports, 1215 Jefferson Davis Highway, Suite 1204, Arlington, VA 22202-4302, and to the Office of Management and Budget, Paperwork Reduction Project (0704-0188) Washington DC 20503.			
1. AGENCY USE ONLY *(Leave blank)*	**2. REPORT DATE** December 2010	**3. REPORT TYPE AND DATES COVERED** Master's Thesis	
4. TITLE AND SUBTITLE Disturbance Detection in Snow Using Polarimetric Imagery of the Visible Spectrum		**5. FUNDING NUMBERS**	
6. AUTHOR(S) West, David C. (LCDR)			
7. PERFORMING ORGANIZATION NAME(S) AND ADDRESS(ES) Naval Postgraduate School Monterey, CA 93943-5000		**8. PERFORMING ORGANIZATION REPORT NUMBER**	
9. SPONSORING /MONITORING AGENCY NAME(S) AND ADDRESS(ES) N/A		**10. SPONSORING/MONITORING AGENCY REPORT NUMBER**	
11. SUPPLEMENTARY NOTES The views expressed in this thesis are those of the author and do not reflect the official policy or position of the Department of Defense or the U.S. Government. IRB protocol number: N/A.			
12a. DISTRIBUTION / AVAILABILITY STATEMENT Approved for public release; distribution is unlimited		**12b. DISTRIBUTION CODE**	

13. ABSTRACT (maximum 200 words)

Optical polarimetric data were analyzed to determine their utility for detecting disturbances in snow. Research for this thesis was conducted in March of 2010 at Lake Tahoe in various settings and snow depths. Images of footprints, snowmobile tracks, and other disturbances were captured by Bossa Nova's linear stokes polarization camera named SALSA. This device implemented a fast switching liquid crystal polarizing filter to separate polarized light onto a 782 x 582 pixel detector operating in the 400 to 700 nanometer range. The data were then analyzed for polarimetric signatures by isolating the disturbances from the background and then comparing standard deviations of intensity and polarization occurrences. Additionally, texture filters were applied to determine if the disturbances could be enhanced and thus highlighted from the background. The results of the study showed that intensity was a stronger discriminant for disturbances in snow than polarization in the visible spectrum. This result was most likely due to the Umov Effect where bright objects typically have low polarization signatures. This conclusion discounts the significant polarization observed in shadowed regions due to polarized skyshine.

14. SUBJECT TERMS Snow, Polarization, Polarimetric, Disturbance Detection.			**15. NUMBER OF PAGES** 91
			16. PRICE CODE
17. SECURITY CLASSIFICATION OF REPORT Unclassified	**18. SECURITY CLASSIFICATION OF THIS PAGE** Unclassified	**19. SECURITY CLASSIFICATION OF ABSTRACT** Unclassified	**20. LIMITATION OF ABSTRACT** UU

NSN 7540-01-280-5500

Standard Form 298 (Rev. 2-89)
Prescribed by ANSI Std. 239-18

THIS PAGE INTENTIONALLY LEFT BLANK

Approved for public release; distribution is unlimited

DISTURBANCE DETECTION IN SNOW USING POLARIMETRIC IMAGERY OF THE VISIBLE SPECTRUM

David C. West
Lieutenant Commander, United States Navy
B.S., United States Naval Academy, 2001

Submitted in partial fulfillment of the
requirements for the degree of

MASTER OF SCIENCE IN APPLIED PHYSICS

from the

NAVAL POSTGRADUATE SCHOOL
December 2010

Author: David C. West

Approved by: Richard C. Olsen
Thesis Advisor

Colonel David M. Trask, USAF (Ret.)
Second Reader

Andres Larraza
Chairman, Department of Physics

THIS PAGE INTENTIONALLY LEFT BLANK

ABSTRACT

Optical polarimetric data were analyzed to determine their utility for detecting disturbances in snow. Research for this thesis was conducted in March of 2010 at Lake Tahoe in various settings and snow depths. Images of footprints, snowmobile tracks, and other disturbances were captured by Bossa Nova's linear stokes polarization camera named SALSA. This device implemented a fast switching liquid crystal polarizing filter to separate polarized light onto a 782 x 582 pixel detector operating in the 400 to 700 nanometer range. The data were then analyzed for polarimetric signatures by isolating the disturbances from the background and then comparing standard deviations of intensity and polarization occurrences. Additionally, texture filters were applied to determine if the disturbances could be enhanced and thus highlighted from the background. The results of the study showed that intensity was a stronger discriminant for disturbances in snow than polarization in the visible spectrum. This result was most likely due to the Umov Effect where bright objects typically have low polarization signatures. This conclusion discounts the significant polarization observed in shadowed regions due to polarized skyshine.

THIS PAGE INTENTIONALLY LEFT BLANK

TABLE OF CONTENTS

THIS PAGE INTENTIONALLY LEFT BLANK

LIST OF FIGURES

THIS PAGE INTENTIONALLY LEFT BLANK

LIST OF TABLES

THIS PAGE INTENTIONALLY LEFT BLANK

LIST OF ACRONYMS AND ABBREVIATIONS

ASM – Angular Second Momentum

CCD – Charge Coupled Device

DOLP – Degree of Linear Polarization

EM – Electromagnetic

GLCM – Grey Level Co-Occurrence Matrix

GSM – Grey-tone Spatial-Dependence Matrix

IDL – Interactive Data Language

IED – Improvised Explosive Device

ITT VIS – ITT Visual Information Systems

NPS – Naval Postgraduate School

RIS – Regions of Interest Separability

ROI – Region of Interest

USB – Universal Serial Bus

THIS PAGE INTENTIONALLY LEFT BLANK

ACKNOWLEDGMENTS

I give many thanks to Professor Olsen and the staff of the Remote Sensing Center. They provided me with the tools, knowledge, money, and assistance necessary to complete this thesis. I also thank my brother Brian West in providing assistance at the research site and for volunteering to carry the heavy equipment while trudging through the deep snow of Tahoe, CA.

THIS PAGE INTENTIONALLY LEFT BLANK

I. INTRODUCTION

In the scientific and intelligence realms, physical access to an object being studied is sometimes impossible. However, by leveraging all aspects of electromagnetic spectrum (including intensity, wavelength, coherence, and polarization) it is possible to gain a great deal more of information than what the naked eye can detect. While there are many information objectives that scientists and intelligence specialists are trying to achieve, one particularly interesting goal is that of detecting disturbances or aberrations within a static picture. Using sensors capable of detecting the polarized state of light, as well as computer algorithms to analyze the data, it is possible to "pull out" and isolate regions of interest that can show these aberrations. The recent advances in computing power and software development now make it practical to use polarized imagery in both scientific and intelligence pursuits.

Detecting disturbances in snow has many practical applications for intelligence communities. The ability to observe a scene from a distance and detect indications of movement, man-made objects, and buried objects provides analysts with valuable planning data necessary for successful intelligence and operational activities. This capability greatly increases the quality of information used in decision-making involving delicate or critical situations.

One focus area that has not been studied in depth is the use of polarization to detect disturbances in snow. The lack of study in this field is due to the relatively low levels of polarization typically seen from snow surface reflections, and the fact that the naked eye can typically see these disturbances by utilizing the natural change in intensity (caused by shadows). However, the small changes in polarization can now be enhanced using the aforementioned algorithms and high-power computers and may be used as a method to detect the disturbances

The research for this thesis was conducted in the early months of 2010 in Tahoe, CA. Tracks in snow were created and then imaged by a recently developed camera capable of detecting polarization in the visible spectrum. Next, the images were

processed and analyzed using numerous techniques and algorithms to determine if the changes in polarization were more pronounced than that of intensity. This thesis seeks to describe this research process and to provide a brief background in the underlying physics associated with disturbance detection using polarimetry.

II. BACKGROUND

A. GENERAL HISTORY

Light is an electromagnetic wave phenomena that can be characterized by its intensity, wavelength, coherence, and polarization. While the human eye is capable of detecting the first three of these characteristics to some degree, it is unable to sense light's polarization. It was only in the last few hundred years that humans became aware of and able to detect the polarization of light (Andreou, 2002).

The study of polarization started in 1669, when Danish professor Erasmus Bartolinus first recorded an observation that light became polarized as it passed through Iceland spar—a variety of calcite crystal (Andreou, 2002). Later, in 1808, prominent French army engineer Etienne Louis Malus worked on Huygen's wave theory of light and discovered that unpolarized light became polarized upon reflection off a smooth surface (O'Conner & Robertson, 1997). A year after Malus' discovery, the French astronomer D.F.J. Arago discovered that light from the sky was partially polarized and also determined at what angle the sun would provide the maximum amount of polarization (Coulson, 1992).

One of the most well known qualitative results regarding polarization is that of Brewster's angle. Sir David Brewster, a self-taught scientist and inventor, was deeply interested in polarized light and sought to improve upon Malus's work. In 1815, he discovered the relation between polarization angle and the refractive indices of materials in which they traversed (Brewster, 1815). Coulson accurately defines Brewster's angle:

> Light which is reflected at a certain angle, the polarizing angle, from a smooth surface of a dielectric such as glass or water, is strongly polarized. In fact, the polarization of this reflected light approaches 100%. The tangent of the polarizing angle is the [ratio of the] index of refraction of the reflecting material [to the incident material]. (Coulson, 1992)

Once it was well understood that light had a polarized nature, it was necessary to describe and quantify it. George Stokes, an Irish scientist most famed for his work in hydrodynamics, began to study the nature of light and in 1852 characterized and

quantified the state of polarization. Stokes found that the overall polarization of a combination of independent polarized streams could be described by four constants (which later became known as Stokes Vectors). He then stated that any two light streams with the same value of constants could be seen as optically equivalent.

Brewster and Stokes' research may have a tremendous impact on remote sensing. The ability to detect the amount and type of polarization in electromagnetic waves reflecting off surfaces provided new ways to extract information about those surfaces from a distance. As detectors became more sensitive and computer algorithms faster, scientists and intelligence specialists are able to find (and infer) much information about these distant objects and their surrounding environment. The physical theory behind how remote sensing uses polarization is found in the next section.

B. NATURE OF POLARIZATION

1. Wave Equation and Polarization of Waves

James Clerk Maxwell, a Scottish physicist in the 19th century, developed the electromagnetic theory of light. By combining Gauss's Law, Gauss's Law of Magnetism, Faraday's Law of Induction, and Ampere-Maxwell's law, he was able to create a unified theory of electromagnetism that formed the basis for all electric and magnetic phenomena (Serway, 1998). These four equations are:

$$\oint \vec{E} \bullet d\vec{A} = \frac{Q}{\varepsilon_0} : \text{ Gauss's Law}$$

$$\oint \vec{B} \bullet d\vec{A} = 0 : \text{ Gauss's Law of Magnetism}$$

$$\oint \vec{E} \bullet d\vec{s} = -d\frac{\Phi_B}{dt} : \text{ Faraday's Law of Induction}$$

$$\oint \vec{B} \bullet d\vec{s} = \mu_0 I + \varepsilon_0 \mu_0 \frac{d\Phi_E}{dt} : \text{ Ampere-Maxwell Law}$$

Maxwell used his unified theory to show that a time-dependent electric and magnetic field must satisfy the general wave equation (Serway 1998)

$$\nabla^2 \psi = \frac{1}{v^2} \frac{\partial^2 \psi}{\partial t^2}$$

where ψ represents either field. Using this wave equation and the Ampere-Maxwell law, he found that electric and magnetic fields could be varied in such a way as to constitute a harmonic wave and thus discovered the existence of electromagnetic waves. Maxwell described such waves by assigning the electric field and magnetic field components the following equations:

$$\vec{E} = E_0 e^{i(\vec{k} \cdot \vec{r} - \omega t)} = E_0 \sin(\vec{k} \cdot \vec{r} - \omega t + \varphi_0)$$

$$\vec{B} = B_0 e^{i(\vec{k} \cdot \vec{r} - \omega t)} = B_0 \sin(\vec{k} \cdot \vec{r} - \omega t + \varphi_0)$$

where $\vec{k}$ is the direction of propagation ($k = 2\pi / \nu =$ propagation constant), ω is the angular frequency of the wave ($\omega = 2\pi\nu$) and φ is the phase of the wave (Pedrotti & Pedrotti, 1993). It should be noted that the electric and magnetic fields are always perpendicular to each other as well as to the propagation vector that is shown in Figure 1.

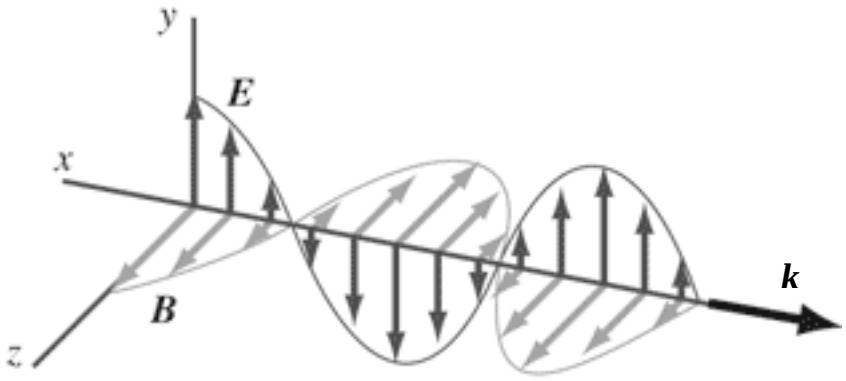

Figure 1. Electromagnetic Wave Example (After WikiPremed MCAT Course, http://wikipremed.com/01physicscards600/405a.gif, 2010)

2. Superposition and Types of Polarization

Like most waves in nature, electromagnetic waves adhere to the principle of superposition. This principle states that a wave can be defined as the sum of the constituents of separate waves (Pedrotti & Pedrotti, 1993). The constituents can be the electric field amplitude, the magnetic field amplitude, or the polarization state. Using the

principle of superposition, one can break down a complicated EM waveform into a set of more basic waves or, vice-versa, create a complicated wave from simpler ones. Figure 2 shows an E-vector combination of two waves travelling in the z-direction (one wave oscillating in the x-direction and one oscillating in the y-direction) resulting in a wave with an electric field oriented at some instantaneous off-axis angle.

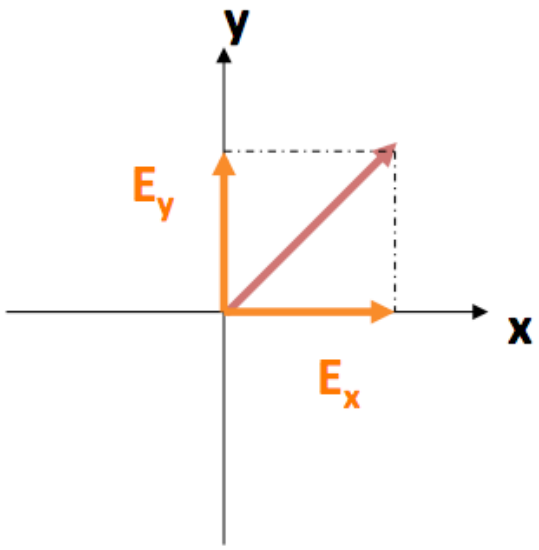

$$\vec{E} = \hat{i}E_{ox}e^{i(kz-\omega t+\varphi_x)} + \hat{j}E_{oy}e^{i(kz-\omega t+\varphi_y)}$$

Figure 2. Superposition of Two Wave's E-Vectors (From NPS PH3292 Applied Optics course, Professor Andres Larraza)

The principle of superposition is particularly useful in determining and describing the polarized state of light. Mathematically, a wave's polarization describes the orientation of the E-field oscillations in relation to the propagation vector of the wave. The two basic states of polarization are described in relation to an arbitrary x-y coordinate system and are known as linear horizontal and vertical states. All other polarization states can be defined by the superposition of these two as well as the difference in their phases (see Figure 3). The combination of two or more waves with differing polarization states and phases can produce an infinite set of polarization possibilities. The most common combinations are circular ($\Delta\phi = \pi/2$), elliptical

($\Delta\phi \neq 0$), and linear ($\Delta\phi = 0$) which are depicted in Figure 3. If two or more waves of varying polarized states and random phases are combined, the result is a wave with an unpolarized state (Pedrotti & Pedrotti, 1993).

As stated above, the polarization of a wave is described by the orientation of the electric field in the plane perpendicular to the propagation vector. The electric field can also be split up into its components along the x and y axes to produce:

$$\vec{E}_x(z,t) = E_{0x}\cos(\omega t - \vec{k}\vec{z} + \varphi_x) \qquad \text{and} \qquad \vec{E}_y(z,t) = E_{0y}\cos(\omega t - \vec{k}\vec{z} + \varphi_y)$$

These equations can be then combined to represent what is known as the polarization ellipse equation, which can describe any state of polarization (Schott, 2009).

$$\frac{E_x^2}{E_{0x}^2} + \frac{E_y^2}{E_{0y}^2} + \frac{-2E_xE_y}{E_{ox}E_{oy}}\cos\phi = \sin^2\phi$$

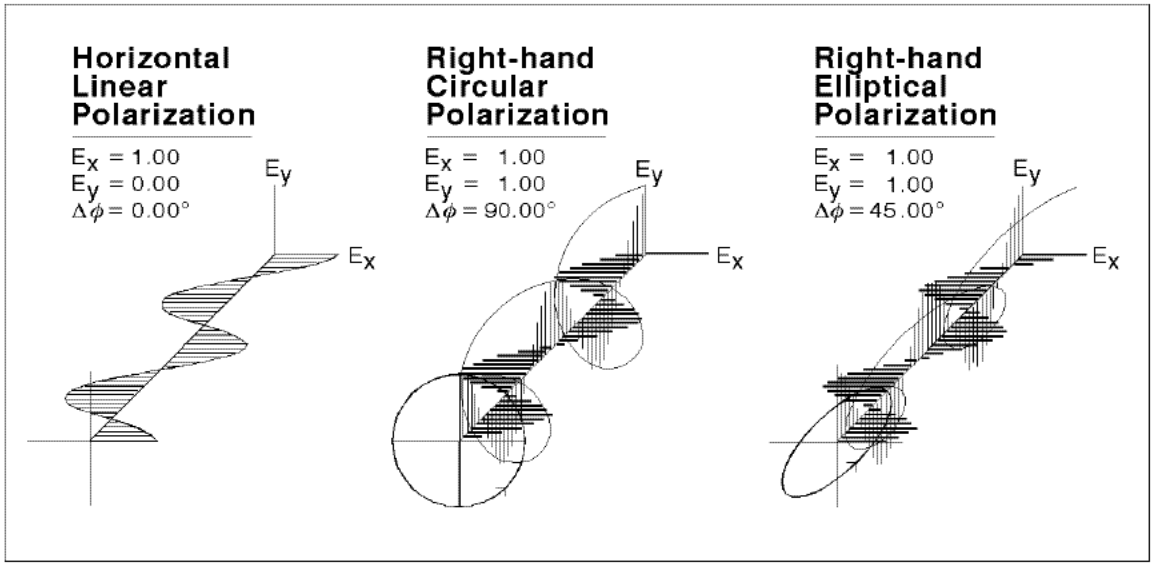

Figure 3. Types of Polarization Due to Superposition (From Brigham Young University, http://www.photonics.byu.edu/polarization.phtml, 2010)

3. Reflection of Light

Polarimetric imagery relies heavily on the interaction between the light source and the surface upon which it reflects. A remote observer can obtain information about these surfaces by detecting the change or lack thereof in the polarization state of a reflected beam. To determine this change, the observer must first predict the expected interactions between the surface and the incident ray. There are three primary concepts that are used to in predicting the polarization of reflected light: The Laws of Reflection and Refraction, Brewster's Angle, and Fresnel Surface Reflections.

The Law of Reflection describes on the macroscopic level how an incident light wave will reflect off a surface that is smooth (or specular) relative to the wavelength of the radiation (Olsen, 2007). A specular surface is one that reflects an incident beam's rays in a uniform direction whereas a diffuse surface is rough and will reflect the rays in various directions (Serway, 1998). Figure 4 shows examples of both types of surfaces. The Law of Reflection states:

> When a ray of light is reflected at an interface dividing two uniform media, the reflected ray remains with the plane of incidence, and the angle of reflection equals the angle of incidence. The plane of incidence includes the incident ray and the normal to the point of incidence. (Pedrotti &Pedrotti, 1993)

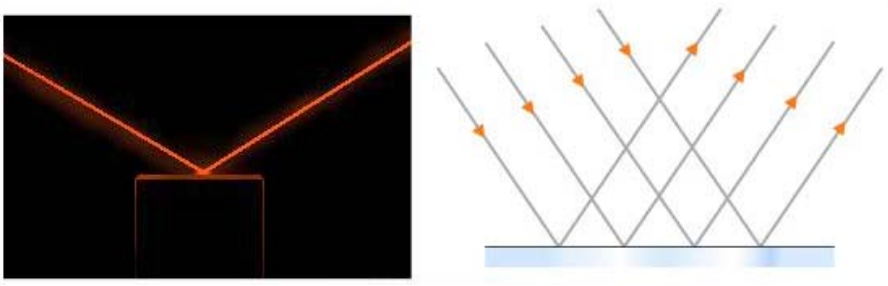

(a)

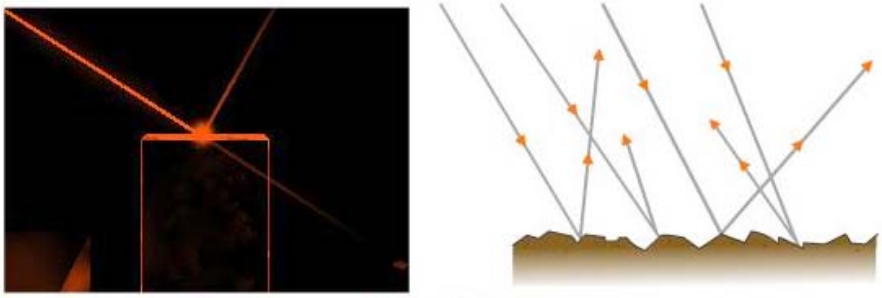

(b)

Figure 4. (a) Specular Reflection from a Smooth Surface (b) Diffuse Reflection from a Rough Surface. (From Tutor Vista, http://www.tutorvista.com/content/science/science-ii/reflection-light/reflection-light.php, 2010)

The law of refraction (also known as Snell's Law) states:

> When a ray of light is refracted at an interface dividing two uniform media, the transmitted ray remains with the plane of incidence and the sine of the angle of refraction is directly proportional to the sine of the angle of incidence. (Pedrotti and Pedrotti 1993)

Snell's Law can be written as:

$$n_1 \sin\theta_1 = n_2 \sin\theta_2 ,$$

where n is the index of refraction of the materials and θ is the angle of the ray with respect to the plane of the surface. It should be noted that the velocity and wavelength of the reflected rays are not altered by either specular or diffuse reflection (Olsen, 2007) but

a phase change does occur if the reflecting media has an index of refraction greater than that of the incident media (Serway, 1998). The relationship between the laws of reflection and refraction is shown in Figure 5.

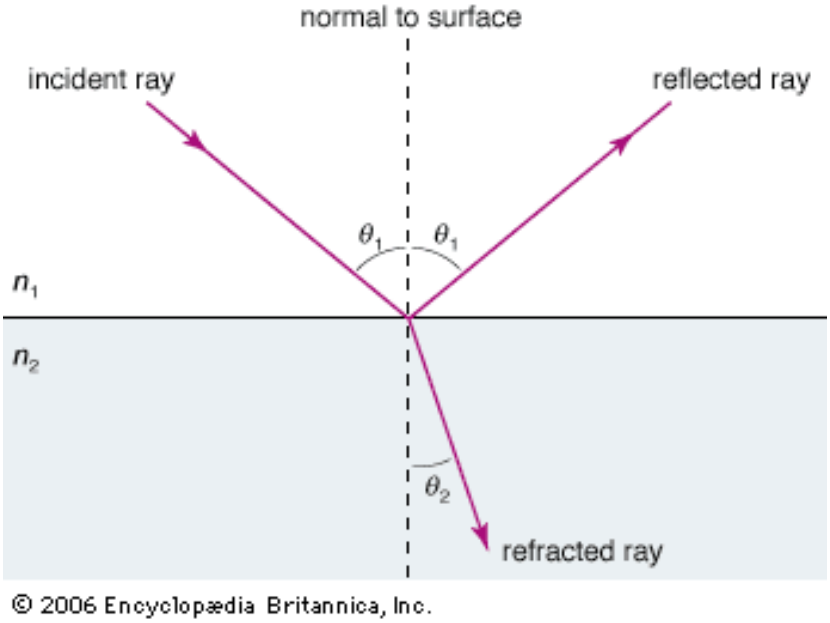

Figure 5. Illustration of Reflection and Refraction Between Two Mediums (From Encyclopedia Britannica, http://media-2.web.britannica.com/eb-media/91/96591-004-959BC455.gif, 2010)

Brewster's Angle was briefly discussed in the previous section and described how the polarization of an incident beam is maximized upon reflection at a specular surface at a specific angle (see Figure 1). This information is extremely important to the remote sensor operator who needs to observe as much polarization as possible in order to detect changes that provides useful target data. As stated by Coulson, Brewster's Angle can be calculated as:

$$\tan\theta_p = \frac{n_2}{n_1} \quad \rightarrow \quad \theta_p = \tan^{-1}\left(\frac{n_2}{n_1}\right)$$

Figure 6 shows an example of Brewster Angle for a light beam propagating in air ($n_1 = 1$) that arrives at an angle of 56.5 degrees from the normal to a surface of smooth glass ($n_2 = 1.513$). Additionally, Brewster found that the total amount of polarized light

in the reflected and refracted beams are equal, but the intensity of the refracted beam is greater. Thus, the refracted beam has a lower degree of polarization (Coulson, 1992). This difference in polarization can be seen in Figure 7.

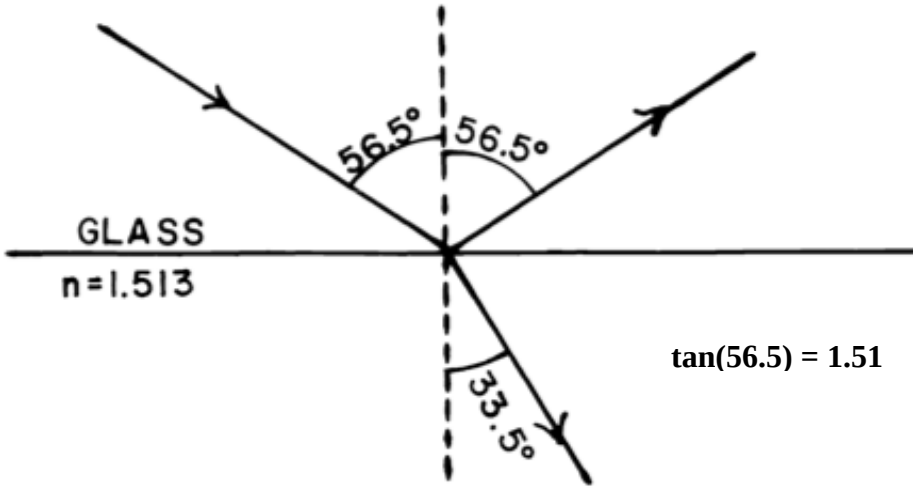

Figure 6. Brewster's Angle for Glass (Image after Coulson, 1992)

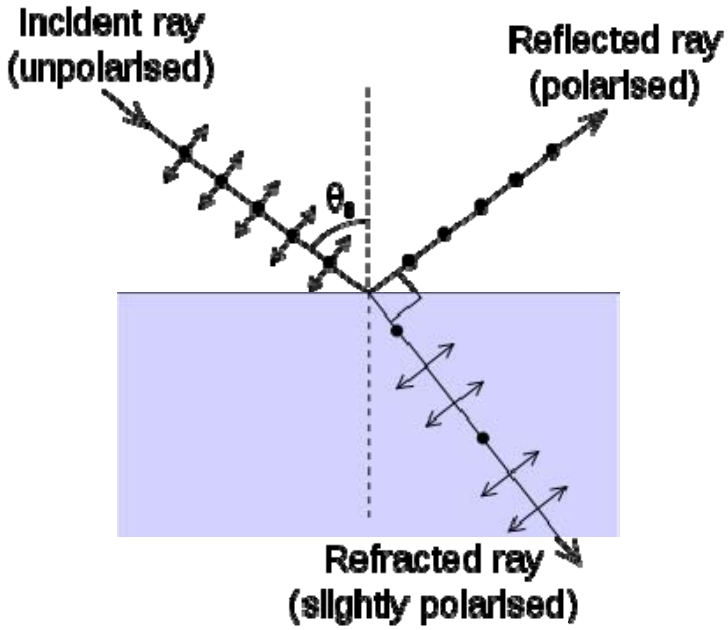

Figure 7. Brewster's Angle and Its Effects (From Wikipedia, http://en.wikipedia.org/wiki/File:Brewsters-angle.svg, 2010)

The last concept involving reflection of light is that of Fresnel Surface Reflections. This concept is important to remote sensing operators as it takes into account the orientation of the radiation's E-vector to reflecting surface's plane of incidence to determine the intensity or amount of energy in the reflected rays. French physicist Augustin-Jean Fresnel showed that the reflectivity of radiation normally incident upon an object with an optically smooth surface (planar dielectric surface) is solely dependent upon the index of refraction of the two media (Schott, 2009). This relationship is seen in the following equation:

$$r^2 = \left(\frac{n_2 - n_1}{n_2 + n_1} \right)^2$$

where r is the reflectivity, n_1 is the index of refraction of the propagation medium, and n_2 is the index of refraction of the reflecting surface. When the incident radiation is not normal to the surface, the orientation of the electric field (i.e. polarization) to the object's dielectric surface must be taken into account. Thus, the equation above becomes the following:

$$r_{\perp} = \left(\frac{n_1 \cos\theta_1 - n_2 \cos\theta_2}{n_1 \cos\theta_1 + n_2 \cos\theta_2} \right) \text{ and } r_{\text{P}} = \left(\frac{n_2 \cos\theta_1 - n_1 \cos\theta_2}{n_2 \cos\theta_1 + n_1 \cos\theta_2} \right)$$

where $\perp$ refers to the electric field being polarized perpendicular to the plane of incidence and || refers to the electric field being polarized parallel to the plane of incidence (Olsen, 2007). Figure 8 graphs the above equations and it shows that reflectivity approaches 100 percent as the incident angle of the radiation approaches 90 degrees. This happens for both parallel and perpendicularly polarized rays. Additionally, Figure 8 shows that incident ray with a polarization that is parallel to the plane of incidence will have little reflection at certain angles which depends on the index of refraction of the two media (Olsen, 2007).

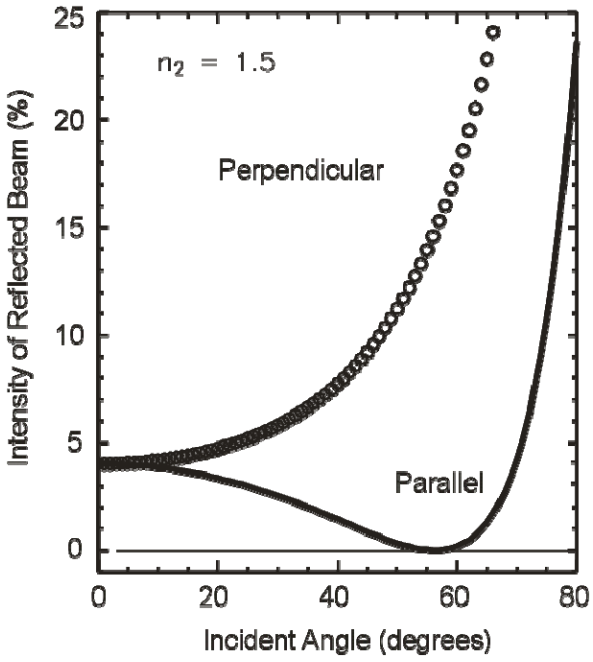

Figure 8. Fresnel Equations. (From Olsen, 2007)

4. Dipoles and Dielectric Mediums

When viewed at the molecular level, the physical properties of reflection become more interesting. A reflecting surface's molecular structure and alignment impacts the type of reflections allowed for both polarized and unpolarized light. Understanding the impact from a reflecting surface's molecular composition is of great importance to the remote sensing operator, as it allows him or her to predict how polarized light will either be reflected or produced. First, it is important to consider what dipoles and dielectric medium are and how they relate to the absorption and production of electromagnetic waves.

A dipole is any molecule where the centers of the positive and negative charge do not coincide (Feynman, 2006). The electric field produced by a dipole is much different that that of a point charge. A point charge's electric field is uniform and radiates infinitely away from the charge in all directions while a dipole creates an electric field that bends in order to maintain field lines that are perpendicular to the equipotential

surfaces (Serway, 1998). The dipoles equipotential surfaces are compressed due to the proximity of unlike charges and can be seen in Figure 9.

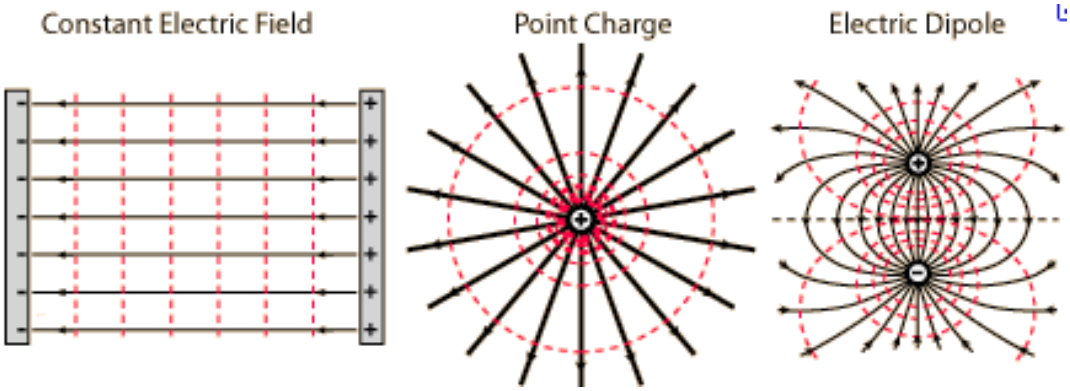

Figure 9. Electric Field Lines Perpendicular to Equipotential Surfaces. (From Georgia State University, http://hyperphysics.phy-astr.gsu.edu/hbase/electric/equipot.html#c3, 2010)

The acceleration of a charge through space alters the electric field lines and thus the radiation pattern. Figure 10 shows a charge accelerating from left to right and the impact upon these fields. Note that the maximum intensity of both the electric and magnetic fields occur perpendicularly (normal) to that of the motion of the charge while they are nearly nonexistent in the direction of motion. Figure 11 shows a charge oscillating up and down and the resultant radiating electric field lines (an EM wave).

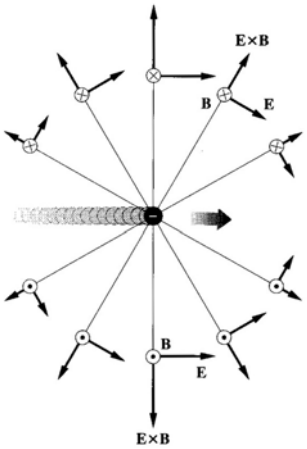

Figure 10. Accelerating Charge and Its Impact Upon the Electric and Magnetic Fields (From Hecht, 2002)

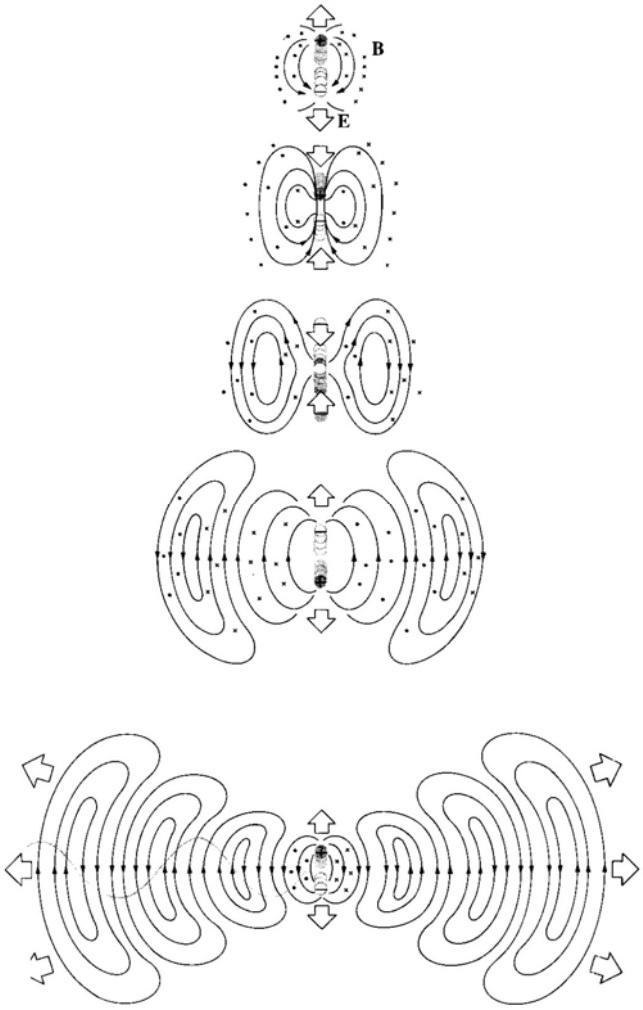

Figure 11. Electric and Magnetic Field Lines Radiated by an Accelerated Charge (From Hecht, 2002)

A simple dielectric is an isotropic material that is nonconducting. An application of an electric field to such a material, whether it consists of polar molecules like H_2O or nonpolar molecules like O_2, shifts the electron cloud with respect to its nucleus and creates a dipole moment. Since electrons behave elastically, there will be an equal and opposite restoring force that will try to return the electrons displaced by the electric field

to their normal state (Pedrotti & Pedrotti, 1993). In the case of polarimetry, the electric field being imposed upon the electron of the reflecting material's molecules is that of the incident light.

Frank and Leno Pedrotti best describe the interaction between dipoles and incident radiation:

> Electromagnetic waves that encounter materials create a complex of interactions with the charged particles of the medium. Forces are exerted on the charges by the electric field of the waves and, because of the motions of the charges, also by the magnetic field of the waves. In responding to these oscillating fields, the charges themselves oscillate and act as radiators of secondary electromagnetic waves. (Pedrotti & Pedrotti, 1993)

Thus, the arrangement of the molecules and the magnitude of the dipole moment within the surface upon which the radiation reflects allow only certain types of reflection. The dipole will only allow specific excitations (or vibrations) and thus will only re-radiate certain types of polarized electromagnetic waves. This is shown in Figure 12, where the molecular dipoles are aligned along an axis very near to the angle of incidence. It can be seen that the transmitted ray's electric field is very strong, since it's propagation vector is normal to the dipole's vibrating axis, and the intensity of the reflected ray's electric field is weaker than that of the incident ray since the molecule's radiation is absent along it's vibrating axis.

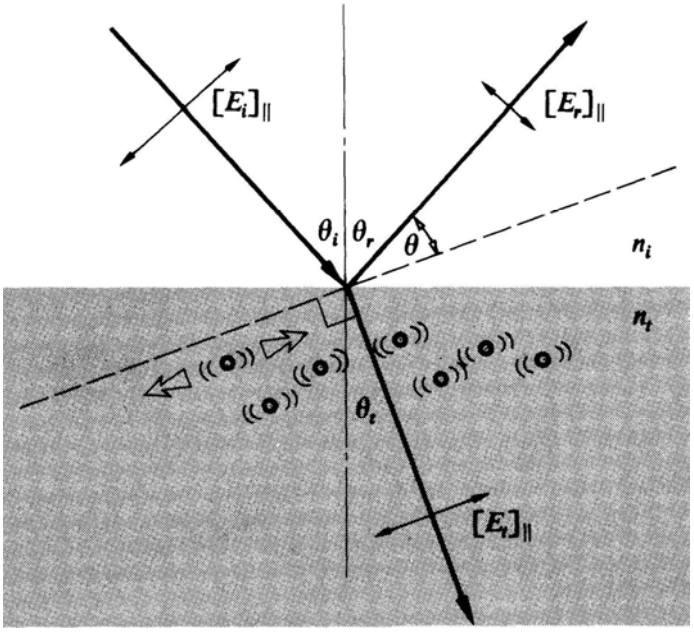

Figure 12. Depiction of Radiation Being Absorbed and Re-Radiated by the Dipoles' Electron Oscillation Within A Reflecting Medium (From Hecht, 2002)

5. Stokes Vectors

The use of Stokes Vectors is a common way of describing the quantity and type of polarization present in radiation. Starting with the polarization ellipse equation and performing some basic algebra manipulation, the following identity is obtained:

$$(E_{0x}^2 + E_{0y}^2)^2 = (E_{0x}^2 - E_{0y}^2)^2 + (2E_{0x}E_{0y}\cos\phi)^2 + (2E_{0x}E_{0y}\sin\phi)^2$$

The four components of this equation are separated to create the four Stokes Vectors:

$$S_0 = E_{0x}^2 + E_{0y}^2$$
$$S_1 = E_{0x}^2 - E_{0y}^2$$
$$S_2 = 2E_{0x}E_{0y}\cos\phi$$
$$S_3 = 2E_{0x}E_{0y}\sin\phi$$

The Stokes Vectors are also known in terms of I, Q, U, and V where:

$$I = S_0$$
$$Q = S_1$$
$$U = S_2$$
$$V = S_3$$

In this representation scheme, I is the intensity, Q is the plane polarization of 0 or 90 degrees, U is the excess of polarized light at 45 or -45 degrees, and V is the amount of circularly polarized light (Egan, 1992).

Now that the Stokes Vectors are defined, an equation to describe the amount of polarization within radiation is needed. The following formula uses Stokes Vectors to describe the amount of polarization (P):

$$P = \sqrt{Q^2 + U^2 + V^2} \; / \; I$$

which equals unity for a polarized state. An alternative metric used to quantify linearly oriented polarization is known as the Degree of Linear Polarization (DOLP) and is defined as:

$$DOLP = \frac{\sqrt{S_1^2 + S_2^2}}{S_0} = \frac{\sqrt{Q^2 + V^2}}{I}$$

C. CHARACTERISTICS OF SNOW

It is important to understand the properties of snow that affect reflection: the permittivity (dielectric constant) and the albedo (Singh & Singh, 2001). However, there is an inherent difficulty in characterizing snow's structural properties since the variations of two mediums of which it is comprised (air and ice) varies greatly in terms of volume, density, temperature, purity, crystal orientation, free water content, etc. (Kuroiwa, 1956).

1. Permittivity of Snow

Snow is a complex substance that consists of air, ice rods, and ice grains that form a three dimensional ice network. It becomes even more complex when water is absorbed which changes the snow from a two element to a three element system (Yosida et al., 1958). The interactions of the internal ice and external electric fields is described as:

> The electric force to which the ice within the snow mass is actually subjected is different from the external electric force applied to the snow. The latter force is modified within snow by the electric interaction which that force induces between one part of the ice network and another. The ice in the snow responds to this modified electric force; the dielectric properties of snow are nothing but the sum total of such responses occurring in every part of the ice network. (Yosida et al., 1958).

The mixture of dielectrics was studied much in the first half of the twentieth century. It was first assumed that the geometry of the electric field of mixed dielectrics was not a function of the relative proportion of the two media. However, this idea was debunked when it was shown that if the particles of the higher permittivity medium elongated in the direction of the electric field then a combined permittivity of the overall substance would be higher then if they were aligned across the field. Thus by varying the proportion of high and low permittivity media within the substance, one can influence the geometry of its electric field (Evans, 1965). This relationship is summarized with the following equation:

$$\frac{\in_m - I}{\in_m + u} = p\left(\frac{\in_1 - I}{\in_1 + u}\right) + (1-p)\left(\frac{\in_2 - I}{\in_2 + u}\right)$$

where $\in_m, \in_1, \in_2$ are the relative permittivities of the mixture and the two constituent media respectively, p is the proportion of the volume occupied by medium one, and I and u are the Formzahl (a parameter describing how one medium is dispersed within another). This equation is important since increasing the permittivity of a substance increases its index of refraction as shown in the following equation:

$$n = \sqrt{\in \mu}$$

Referring back to the formula for Brewster's Angle, a higher index of refraction will increase the angle from the normal in which maximum polarized reflections will occur (or, vice versa, the source radiation must be closer to the plane of incidence to achieve maximum polarization).

However, the permittivity of snow fluctuates greatly. Not only does it vary due the near unlimited varieties and compositions of snow, but it also varies dramatically

throughout the electromagnetic spectrum. Figure 13 shows that the permittivity of a dielectric $\in$ decreases as the frequency of incident radiation increases. In the optical portion of the EM spectrum, the dielectric constant varies anywhere between air (1) and ice (3.2) (Singh & Singh, 2001).

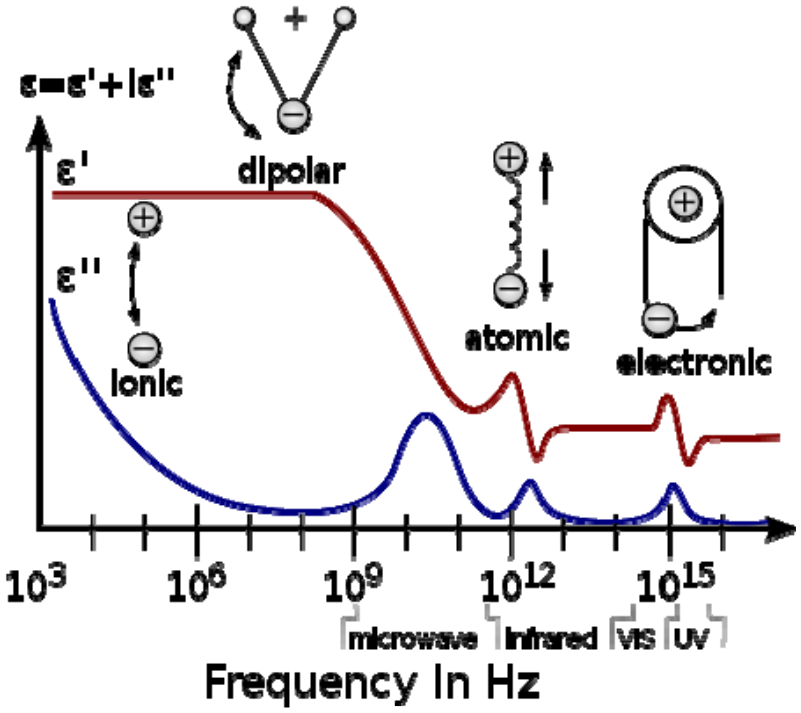

Figure 13. Dielectric Permittivity Over A Wide Range of Frequencies. (From Wikipedia, http://en.wikipedia.org/wiki/File:Dielectric_responses.svg, 2010)

2. Snow Albedo

Albedo is the observable optical parameter that follows from the dielectric constant and the permittivity. It represents the ability of a surface to absorb or reflect radiation where high values indicate reflection and low values indicate absorption. Combining the knowledge of reflected intensity (or brightness) with the Umov Effect (bright reflections have low polarization), one can predict the amount of polarization that will occur upon reflection. Albedo is defined by the ratio of reflected radiation (S_R) to that of the incident radiation (S_I).

$$\alpha = \frac{S_R}{S_I}$$

The amount of reflected solar radiation is impacted by many variables that include solar elevation, depth of snow cover, wavelength, temperature, grain size, and impurities. Additionally, a highly or freshly dusted snow surface will have a lower albedo and reflect less light (Singh & Singh, 2001). Reports show measurements of albedo ranging from 0.29 for porous, dirty, and water saturated to 0.86 when the snow is dry, compact, and clean. For comparison, the mean value of albedo for the Earth's surface is 0.15 (Singh & Singh, 2001). Figure 14 shows the difference in albedo for varying types of frozen water sampled in the Fram Strait.

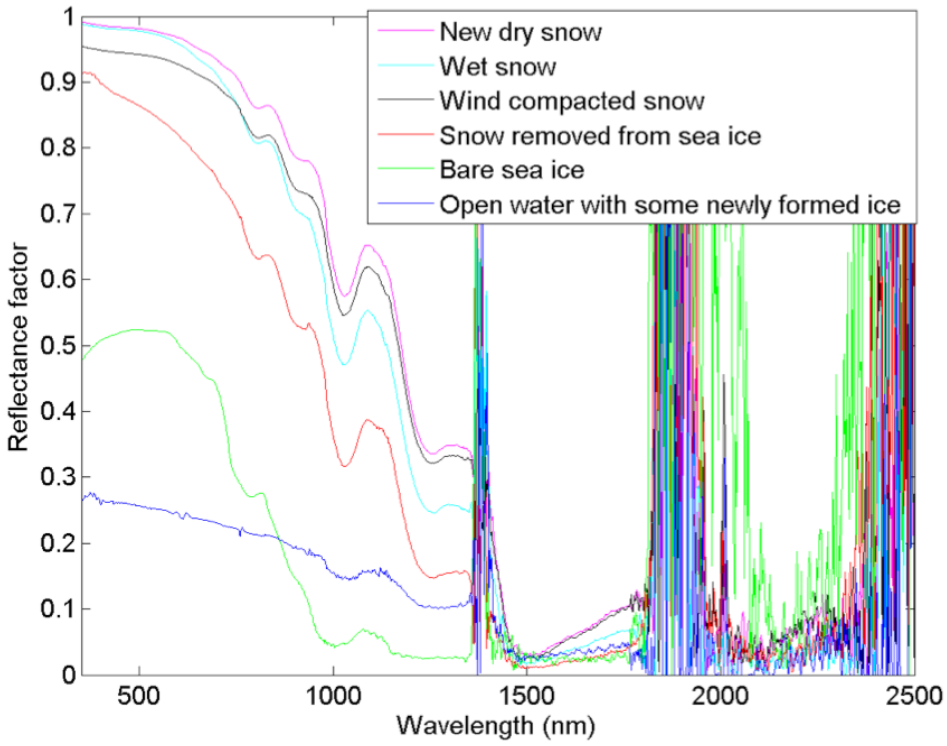

Figure 14. Albedo for Snow Types Sampled in the Fram Strait (From Pedersen, 2007)

D. ADDITIONAL BACKGROUND MATERIAL

There are two important reviews of polarization that led to the creation of this thesis. The first is a book by Dr. John R. Schott titled *Fundamentals of Polarimetric Remote Sensing*. This book provided the author of this thesis with the physical understanding of polarimetry, how to measure and model polarimetric radiation, and the foundations of basic imagery processing used to enhance collected data. The book also describes many scenarios in which polarimetry could be used to gather information not normally obtained by standard cameras such as the composition and roughness of surface materials (Schott, 2009).

The second review is a book by Dr. R.C. Olsen of the Naval Postgraduate School titled *Remote Sensing from Air and Space*. This book provided the author with a high-level understanding of the many remote sensing domains with an added emphasis on military application. It also explained the physical principles associated with each domain and provided explanations of common analysis techniques used to extract useful information from the image data (Olsen, 2007).

E. PREVIOUS NPS RESEARCH

In addition to the reviews of polarization and remote sensing, two Naval Postgraduate School theses provided the background and motivation for this research. The first was Lieutenant Phillip Smith's study of the school's newly acquired polarimetric camera, its ability to detect disturbed surfaces, and other useful capabilities. The second thesis was Ensign Michael Eyler's research that furthered the study of disturbance detection in soils and asphalt to determine if polarization would be useful to detect Improvised Explosive Devices (IEDs). The following sections provide a brief overview of the polarimetric camera and a summary of Smith's and Eyler's research.

1. Imaging Hardware

This research for all three theses was conducted using a linear stokes polarization camera named SALSA that was created by Bossa Nova Technologies. The device includes proprietary software that directly operates the camera, performs mathematical

computations of the Stokes Vectors, and renders polarimetric images in real time for viewing. Figure 15 shows a picture of this camera.

Figure 15. SALSA Camera (From Bossa Nova Technologies Brochure, 2010)

The SALSA camera is housed in a 4" x 4" x 6" aluminum enclosure and utilizes a 782 x 582 pixel Charge Coupled Device (CCD) as its detector. This detector operates in the visible part of the electromagnetic spectrum (400-700 nm) and uses 12 bits to represent the value of each pixel using a monochromatic scale. The camera can handle 35 raw frames per second or 8.75 polarization frames per second while in video mode at max resolution and the aperture can accommodate any standard Nikon F mounted lens. The video setting of the SALSA camera can be used in "live mode" to instantly detect and calculate polarization of a scene. See Table 1 for a more comprehensive listing of SALSA's technical specifications.

Table 1. SALSA Camera Specifications (From Bossa Nova Technologies Brochure, 2010)

SALSA video format	Digital IEEE-1394, 12 bits monochrome, 782x582 pixels
Acquisition Interface	IEEE-1394
Synchronization Interface	USB
Camera Size	4” x 4” x 6” (without lens)
Lenses	Standard Nikon F-mount lenses
Frame rate at max resolution and 12bits mode	35 raw frames per second 8.75 polarization frames per second (movie mode)
Frame rate at 320x240 resolution at 12bits mode	110 raw frames per second 28 polarization frames per second (movie mode)
Spectral Bandwidth	400-700 nm The technology can be adapted to other spectral bands or larger spectral bands
Calibration	Factory calibrated
Laptop Operating System	Windows XP/Vista

Instead of a using a mechanically rotating device to perform polarization filtering, the SALSA camera implements a fast switching liquid crystal polarizing filter to capture the three different polarization states of incoming light. These states are the I, Q, and U Stokes Vectors representing intensity, 0- or 90-degree polarization, and 45- or –45-degree polarization respectively. The technical process of how the SALSA camera captures the different polarizations states is explained by the following:

> The first element is a 45-degree polarization rotator and the second element [is a] 90-degree polarization rotator. The 45-degree polarization rotator is composed of a quarter waveplate and a programmable quarter wave plate. The orientation of the neutral axis of the programmable quarter waveplate is electrically tilted by 45 degrees between the two states. A ±45 degrees linear polarization is converted to a circular polarization after the first waveplate and converted again to linear

polarization after the second quarter wave plate. The 90-degree polarization rotator is composed of a programmable half wave plate. The orientation of the neutral axis of the programmable half waveplate is electrically tilted by 45 degree between the two states. Combined together, these elements give access to 4 states of polarization which are -45°, 0°, 45° and 90°. (Lefaudeux, Lechocinski, Breugnot, & Clemenceau, 2007).

Figure 16 provides a visual example of how SALSA performs polarization filtering using a modulator.

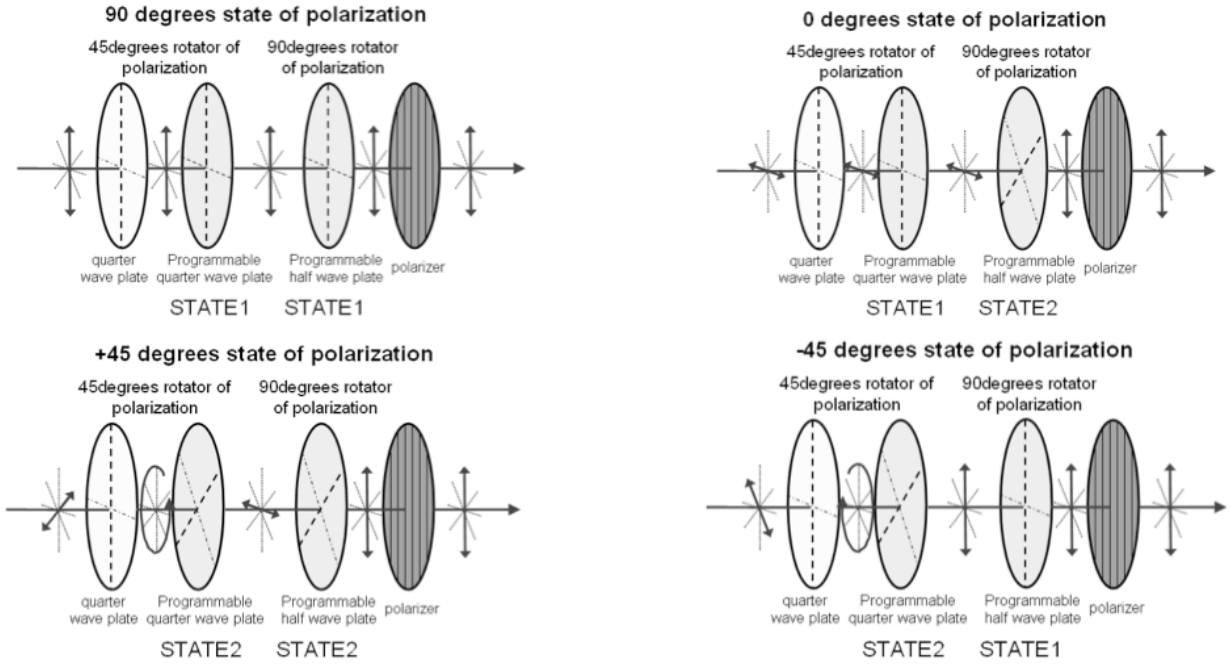

Figure 16. SALSA Polarization Modulator Principle (From Lefaudeux, Lechocinski, Breugnot, & Clemenceau, 2007)

A tripod, portable power supply, laptop with firewire (IEEE-1394) and USB connections, and appropriate data cables are required for fieldwork. The power supply used for conducting this thesis' research was a Duracell Powerpack 600. This battery system is capable of providing ample power for three days of continuous data collection and is extremely portable. Due to the bulky equipment necessary to utilize the SALSA camera properly, it is highly recommend that an assistant be available to help carry the equipment to remote research locations.

2. Initial Studies Using the Polarimetric Camera at NPS

Lieutenant Phillip Smith's thesis titled, "The Uses of A Polarimetric Camera," was the first research at NPS involving the SALSA device. His primary goal was to determine the performance capabilities of the camera and to determine the ability of modern image analysis software to extract useful information from polarimetric data. One of the more interesting results of his research was an image of NPS' administration building, Hermann Hall. Figure 17 is a combination of the original intensity image and the corresponding Degree of Linear Polarization (DOLP) calculation. Figure 18 is the corresponding scatter plot of DOLP and inverse intensity. It depicts the regions of interest selected by the author used to isolate different objects and backgrounds within the image based on their intensity and polarization. Figure 19 is the overlay of these regions of interest onto the intensity image, which allows the observer to find objects producing similar polarization. These last two figures also illustrate the Umov Effect where darker objects have more polarization than lighter objects. Note the linear relationship between inverse intensity and DOLP.

Figure 17. Hermann Hall Image on August 1st, 2008. Intensity (left) and DOLP (right) (Images from Smith, 2008)

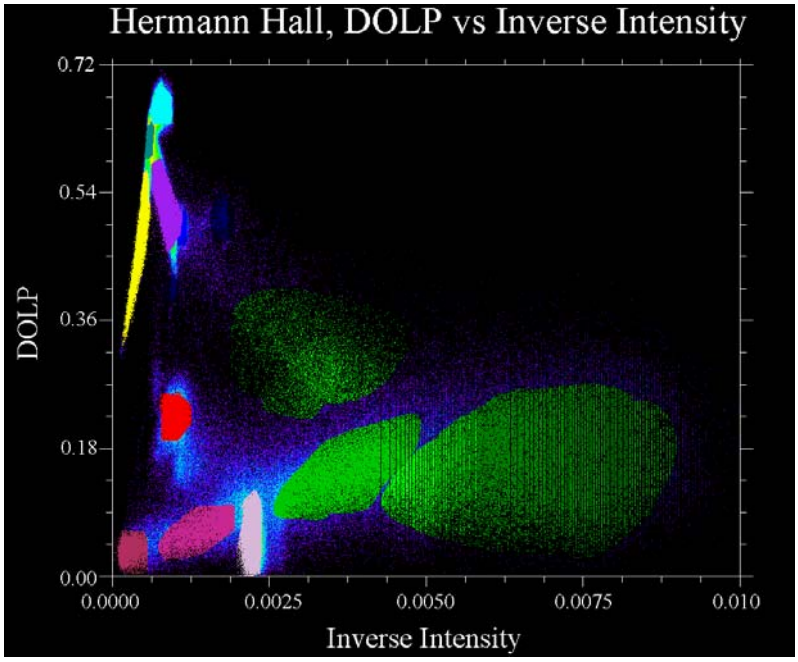

Figure 18. Hermann Hall Regions of Interest (From Smith, 2008)

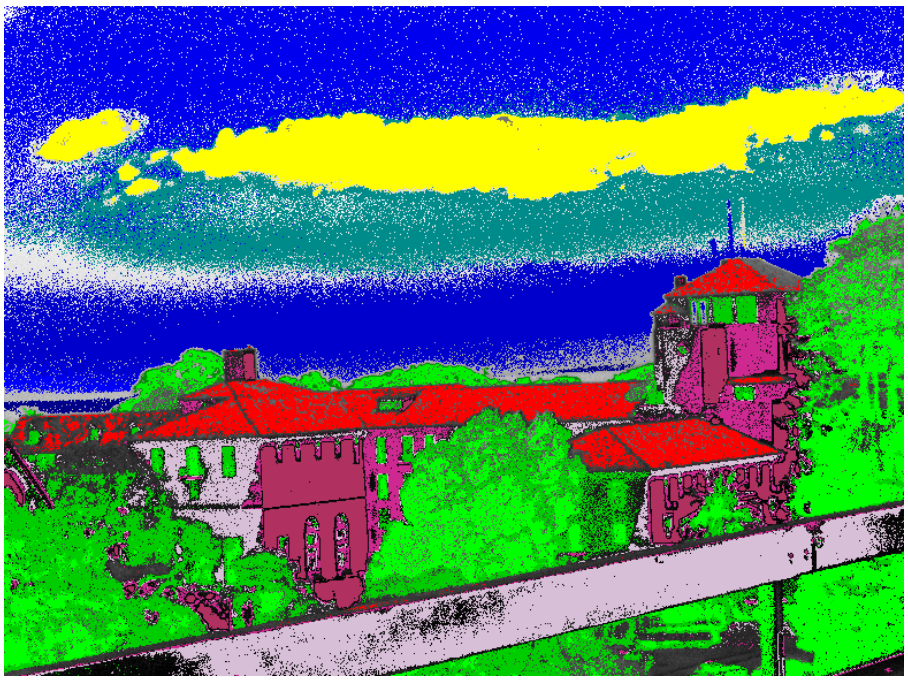

Figure 19. Hermann Hall Region of Interest Overlay (From Smith, 2008)

3. Applications to IED Detection

The second thesis involving the SALSA camera was that of Ensign Michael Eyler, USN. His thesis titled, "Polarimetric Imaging for the Detection of Disturbed Surfaces," (2009) sought to explore the utility of polarimetry in protecting U.S. servicemen from the dangers of IEDs. His thesis investigated many types of surfaces such as asphalt (rough, freshly paved, and dug-up varieties), sand, and dirt to see if polarimetric data could be used to detect unusual disturbances. Figure 20 is an excerpt of his research and shows an analyzed image of a parking lot with recent repairs (patching) that has a detectable polarization difference between disturbed and undisturbed asphalt. The blue pixels indicate the likelihood that the asphalt at that location is disturbed and the red pixels indicate the likelihood that the asphalt is undisturbed. The overall results of his thesis concluded that polarization provided moderate capability to detecting disturbed asphalt surfaces but disturbed soils were less than expected (Eyler, 2009).

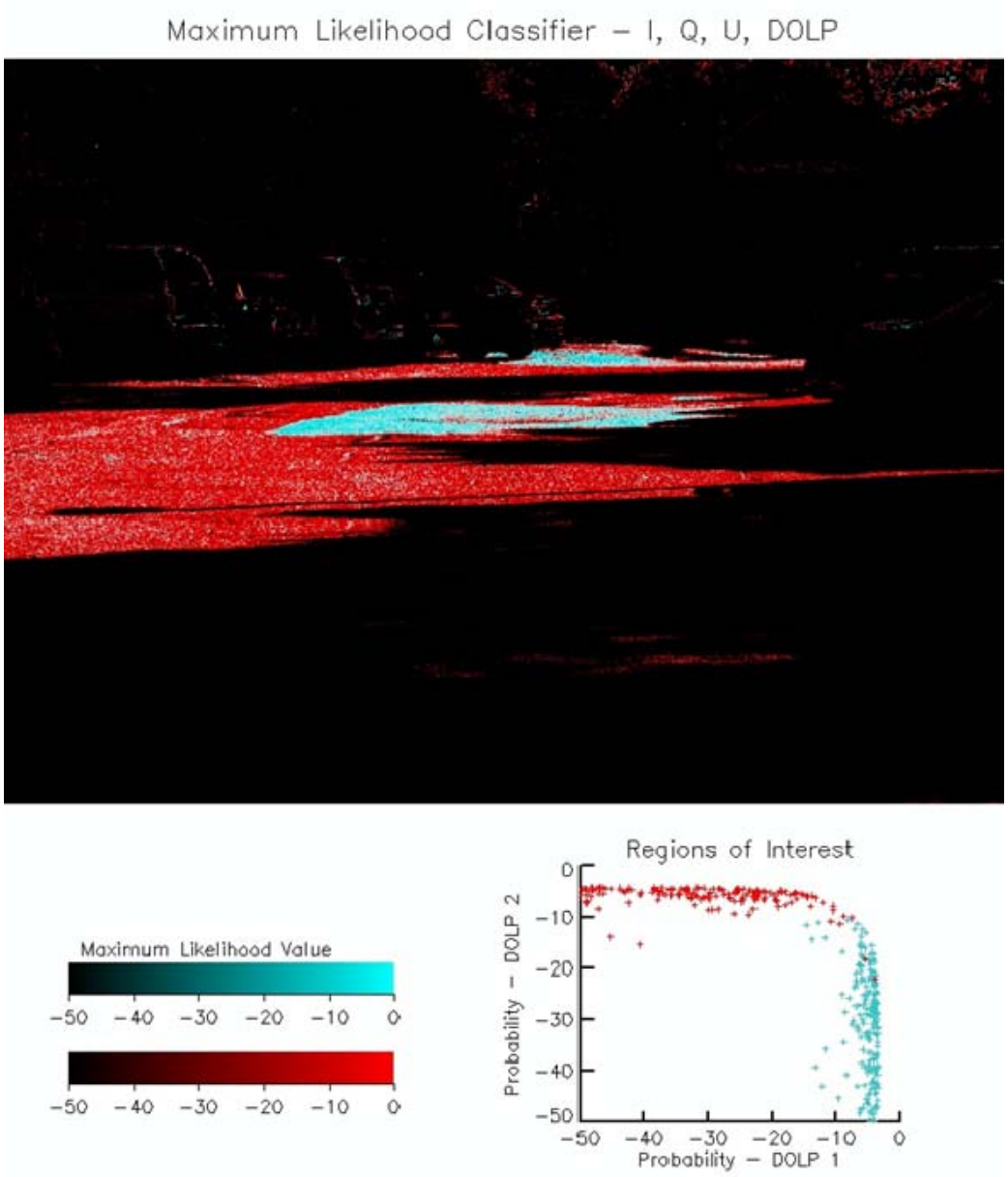

Figure 20. Parking Lot Image Analyzed by ENVI's Maximum Likelihood Classifier. Disturbed Asphalt (blue) and Undisturbed Asphalt (red). (From Eyler, 2009)

THIS PAGE INTENTIONALLY LEFT BLANK

III. PROBLEM

A. HYPOTHESIS

Intelligence analysts need the ability to observe distant objects and to gather as much data as possible so that it can be transformed into useful information. One such piece of information they need is the type and amount of disturbances within a scene. This information can indicate possible activity, movement, man-made objects, or other natural forces that impact the surroundings. In a typical image, the naked eye relies on color and intensity to detect these disturbances but camouflage and very bright environments such as snow can make this a difficult task. Polarization data provides this information since disturbed and man-made surfaces polarize light differently then the surrounding environment.

Snow is a unique surface that makes detecting disturbances more difficult than in other environments. Reflections of both disturbed and undisturbed snow are relatively bright and it is difficult to find disturbances using intensity alone. However, according to the Umov Effect, bright surfaces tend to have mostly unpolarized reflections while dark surfaces tend to have highly polarized reflections (Schott, 2009). Thus, disturbances in the snow or objects camouflaged white will have little change in intensity in the visible spectrum and consequently the change in polarization may be too small for normal detection purposes. However, using advanced imagery processing software, objects or disturbances that produce these small changes in polarization could be enough to allow for their detection. Additionally, the pressure of a footstep, wheel, or track may cause a melting and refreezing that will produce a smoother surface that that of the surrounding snow. This should increase specular reflection enough to provide a larger change in polarization compared to the surrounding snow and thus the disturbance could be detected in a polarized image.

The goal of this thesis is to determine if this polarization data can produce more useful information about disturbances in snow than just that gained by an image of intensity only. By taking numerous images of both disturbed and undisturbed snow at

various angles to an incident light source and then using advanced imagery processing techniques, it is possible to find enough changes in polarization that would give analysts another tool for remote sensing.

B. IMAGING PROCEDURE

The images for this research were taken in Tahoe City, CA, during the late winter season when plenty of snowfall was available. The first set of images was captured at two different locations on March 9, 2010. The first location was at a local hotel with a flat cement patio on top of a one-story garage and the polarimetric camera was situated on an overlooking balcony on the 7th floor. Wide-angle and telephoto zoom lenses were then used to capture images of both clean and tracked snow between the hours of 0900 and 1000. The second location was a nearby public golf course covered in approximately two feet of snow. The golf course served as a public place to snowmobile, walk dogs, snowshoe and hike and was consequently full of useful tracks that could be imaged. However, fresh tracks were made by the research assistant to ensure deep depressions and uniformity. These images were taken between the times of 1150 and 1250 on the same day as the balcony pictures and the temperature stayed at 24 degrees Fahrenheit for both collection periods.

The second set of images was taken on March 11th, 2010 between 0900 and 1100 local time and only the wide-angle lens was used. The golf course was used again since over 2 inches of precipitation fell the night before which provided an excellent opportunity to image freshly fallen snow. By 0900, snowmobile tracks and footprints were already available for data collection. The air temperature during the image collection varied between 35 and 42 degrees.

The National Oceanographic and Atmospheric Administration's Solar Position Calculator (http://www.srrb.noaa.gov/highlights/sunrise/azel.html) was used to determine the sun's elevation at the research sites. Plugging in coordinates found on Google Earth (39.172135N, 120.142418W) and the times the images were taken into the calculator, determined that the Sun's elevation in the sky to be between 40 and 48 degrees from the horizon. The solar azimuth was near 172 degrees.

Since Fresnel Reflection and Brewster's Angle are highly important in polarization, the camera was placed directly opposite the Sun (180 degrees) in relation to the snow being imaged. Additionally, as a measure of experiment control, the images of the same scene were taken at 0, 90, and 180 degrees in relation to the Sun. This was to see if there would be any polarization from the scattering effects of coarse snow or to see if the partially polarized light from the atmosphere would reflect and produce a detectable signature as well.

C. ANALYSIS TECHNIQUES

Analysis of the data collected by the SALSA camera was done using ITT Visual Information Systems' (ITT VIS) geospatial imagery processing software known as ENVI. Inside ENVI, Haralick texture filters and Regions of Interest Separability (RIS) were the primary algorithms applied to extract useful information from the data. ENVI's accompanying programming language, known as the Interactive Data Language (IDL), was used to provide greater precision of data analysis and graphing.

1. Texture Filters

Haralick, Shanmugam, and Dinstein (1973) define texture as the information pertaining to the spatial distribution of gray tone values within a black and white image. Applying a texture filter first requires the algorithm to assign each pixel in the image a tonal value based on a user defined scale (small ranges cause a loss of resolution while large ranges require more memory and processing power during computation) (Puetz & Olsen, 2006). Next, the algorithm creates a Grey Level Co-Occurrence Matrix (GLCM) that represents the frequency of occurrence in tonal values within a user-defined direction/distance to each pixel in the image. Linear algebra can then be used to manipulate the GLCM in numerous ways to highlight the differences or similarities between neighboring pixels. Finally, this new manipulation can be redisplayed as a new image that can allow the naked eye to better identify the information being sought by the user (Haralick, Shanmugam, & Dinstein, 1973).

Figure 21 shows the directional relationships used in creating a GLCM. Figure 19(a) is an example of a 4x4 pixel image with a gray tone scale of 0-3; Figure 22(b) is

the generalized GLCM for a 4x4 image where the values in parentheses represents a neighbor tone pair and the number of times they occur in that image; and Figures 22(c–f) are the resultant Grey-tone Spatial-Dependence Matrix (GSM) for each of the four primary directions at a separation distance of one.

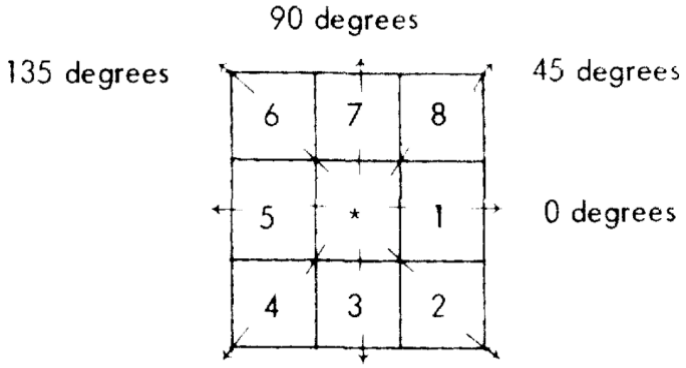

Figure 21. The Directional Relationship Between the Center Pixel and Its Neighbors (From Haralick, Shanmugam, & Dinstein, 1973)

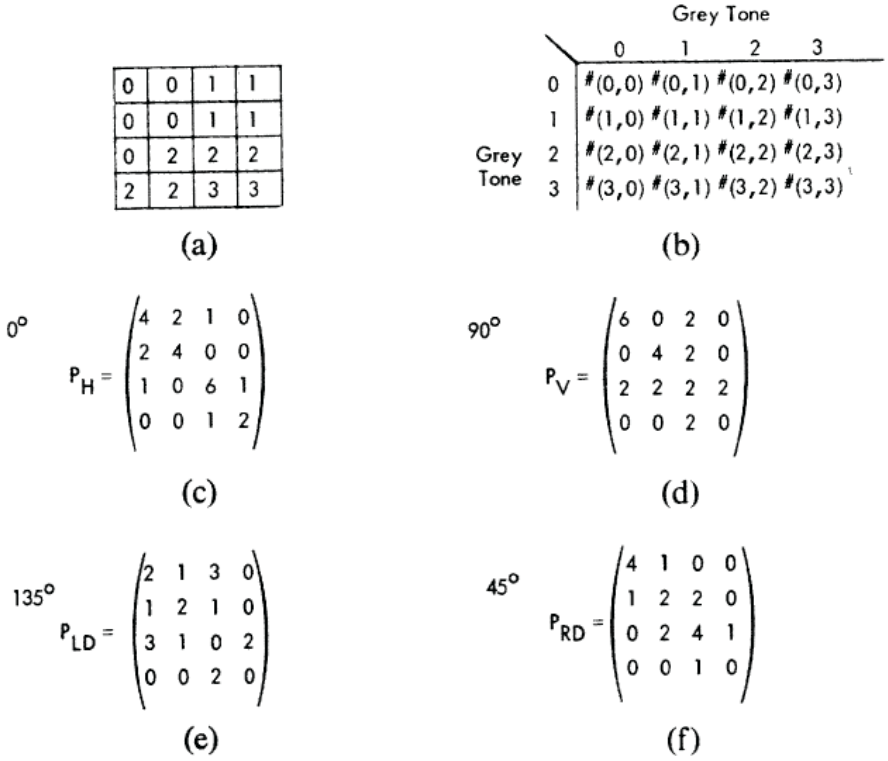

Figure 22. The Four Types of Grey Level Co-Occurrence Matrices Generated from a 4x4 Pixel Image with a Separation Distance of One (From Haralick, Shanmugam, & Dinstein, 1973).

As stated above, the GLCM can be manipulated using linear algebra to highlight relationships between the gray tone values of neighboring pixels. The formulas that were most relevant and useful to this thesis were the ones that calculated the angular second momentum, contrast, correlation, variance, and entropy of the gray tone values within the image. These formulas are shown below where *p(i,j)* represents the normalized *(i,j)*th entry in the GLCM, *N* is the number of distinct gray levels, and $\mu_x, \mu_y, \sigma_x, \sigma_y$ are the means and standard deviations of the marginal distribution of *p(i,j)* (Haralick, Shanmugam, & Dinstein, 1973).

$$\text{Angular Second Momentum} = \sum_i \sum_j \{p(i,j)\}^2$$

$$\text{Contrast} = \sum_{n=0}^{N_{g-1}} n^2 \left\{ \sum_{i=1}^{N_g} \sum_{j=1}^{N_g} p(i,j) \right\}$$

$$\text{Correlation} = \frac{\sum_i \sum_j (ij) p(i,j) - \mu_x \mu_y}{\sigma_x \sigma_y}$$

$$\text{Variance} = \sum_i \sum_j (i-\mu)^2 p(i,j)$$

$$\text{Entropy} = -\sum_i \sum_j p(i,j) \log(p(i,j))$$

2. Regions of Interest Separability

ENVI provides a useful set of tools to take given data and then create regions of interest based on users selected criteria. By creating a 2-D scatter plot of the degree of linear polarization versus the inverse of intensity, groups of similar values become localized (or separated) and identifiable to the analyst. This user can then assign each distinct region with a color and then superimpose that color on the original image. This allows for the easy observation of where similar degrees of polarization are occurring within the scene. Using the IDL associated with ENVI, this data can be normalized and plotted on a histogram to show the frequency of occurrence for the amount of

polarization and/or the value of intensity within the image. This analysis tool is crucial to determining if DOLP is useful for discriminating disturbances from the background when compared to intensity (i.e., what the eye will normally see). The separation in peaks between the background and disturbance indicates the ease of detection of that disturbance. The difference in separation of the peaks in the DOLP and Inverse Intensity curves determines if polarization is better at detecting disturbances compared to intensity images.

IV. OBSERVATIONS AND ANALYSIS

A. HOTEL BALCONY

1. Wide-Angle Image

The first image captured by the polarization camera was the 7th-floor balcony shot on March 9. The previous night's snowfall was thin and beginning to melt but was still useful in the research for this thesis. Due to the shallow depth of the snow and the lack of drainage on the garage roof, the snow had an elevated moisture content. This led to the snow becoming highly compressed and translucent upon being walked on by the research assistant. The original intensity image and the corresponding DOLP image calculated by ENVI can be seen in Figure 23, which shows that the polarization signature of the footsteps can be correlated with the low intensity points (as predicted by the Umov Effect). The texture filters were then applied to the DOLP image and produced the five images shown in Figure 24. While the texture filters served to isolate the polarized areas within the original image, they were not extremely useful over intensity in identifying the disturbances.

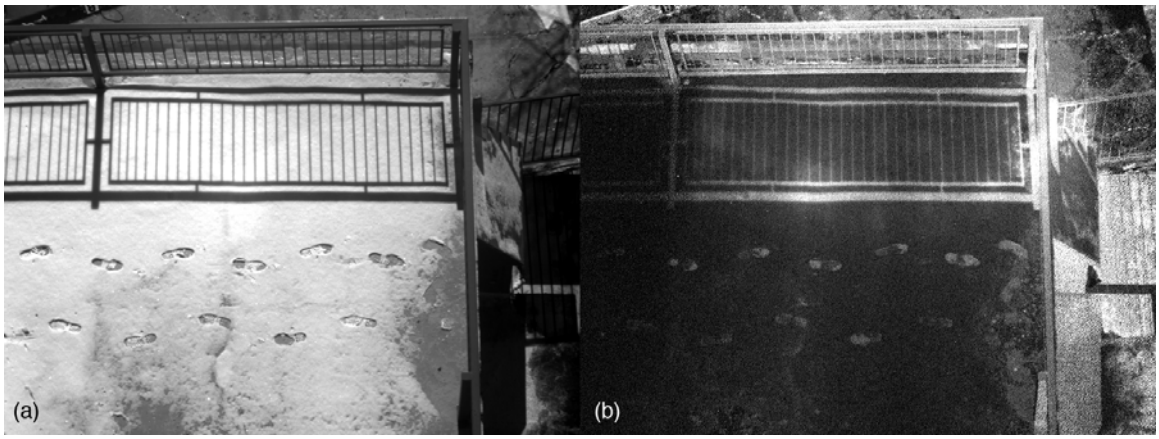

Figure 23. Wide-Angle Image of Disturbed Snow from 7th Story Balcony: (a) Intensity and (b) DOLP.

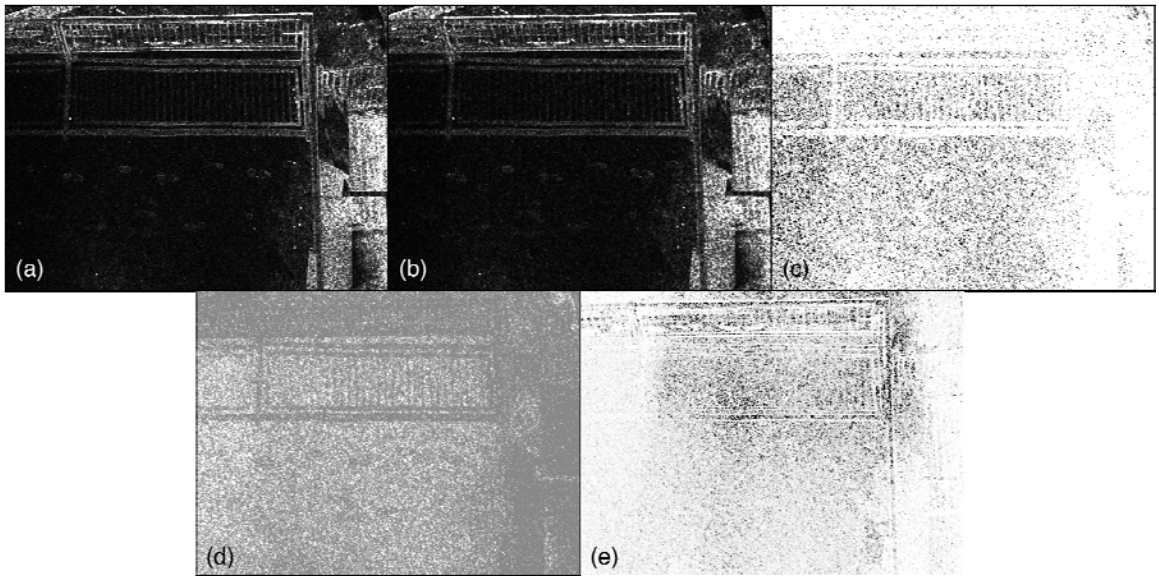

Figure 24. Texture Filters Applied to Wide-Angle Image from 7th Story Balcony: Variance (a), Contrast (b), Entropy (c), ASM (d), and Correlation (e).

After creating the texture images, a scatter plot was created that compared the inverse intensity to the Degree of Linear Polarization in the scene. Prominent regions were detected and then highlighted by the author using a color scheme where red represented undisturbed/background snow and blue represented the disturbed snow. These regions of interest can be seen in Figures 25 and 26. These plots show that there is a distinct and observable polarization difference between the disturbed and undisturbed snow. Figure 27 shows an overlay of these ROIs upon the original intensity image, S0. Two things should be noted about the figures. The first is that the color scheme instituted for disturbed and undisturbed snow was used throughout the analysis portion of this thesis. The second is that great care was taken to remove shadowed pixels from the analysis, as they would otherwise skew results since sky-shine is naturally polarized.

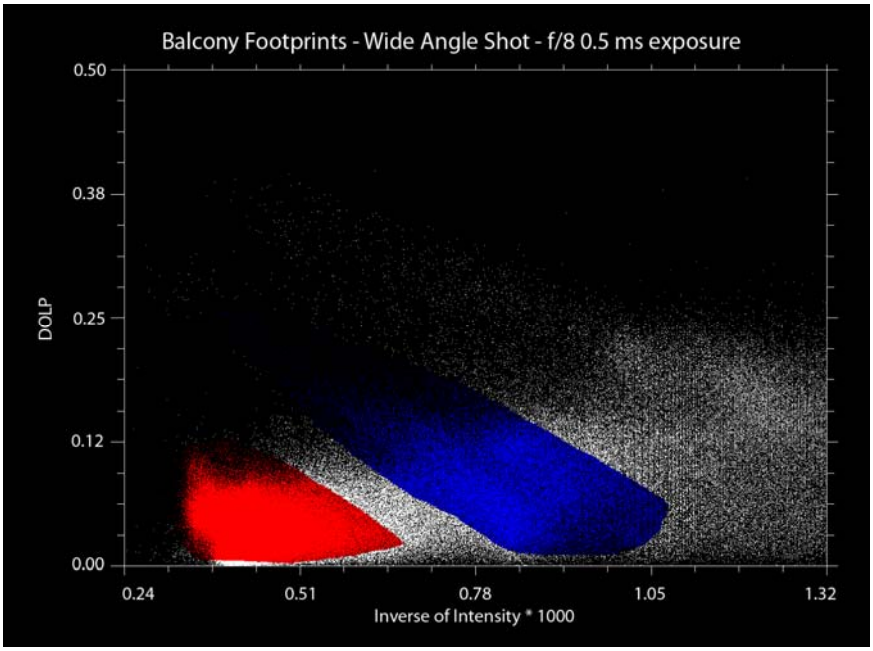

Figure 25. Cropped Scatter Plot of Regions of Interest for the Wide-Angle Balcony Image: Background (red) and Footprints (blue).

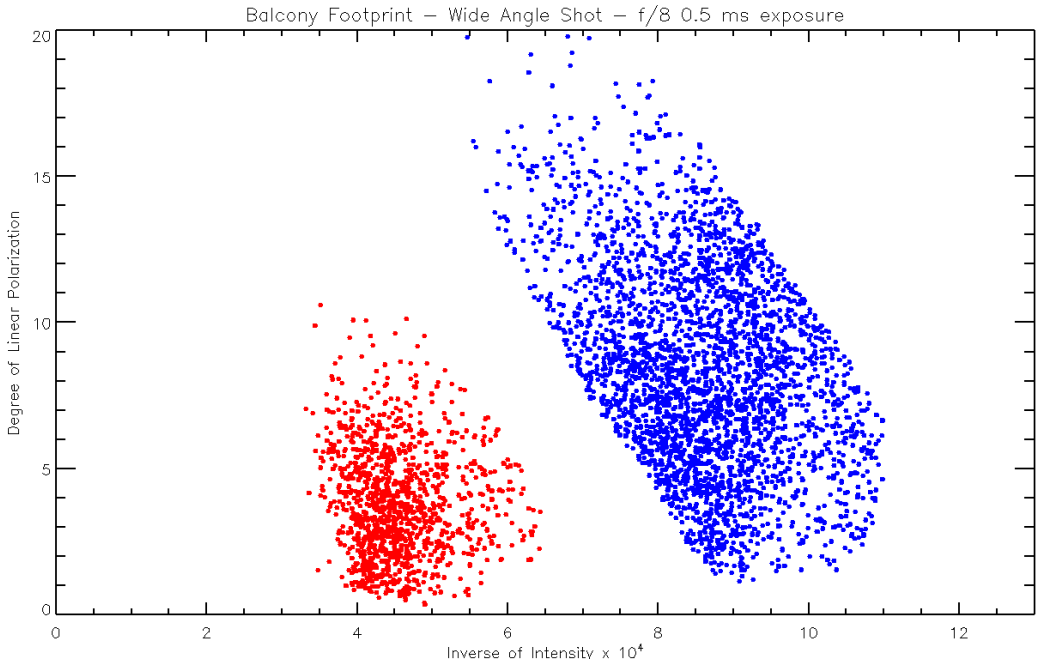

Figure 26. Simplified Scatter Plot of Regions of Interest for the Wide-Angle Balcony Image: Background (red) and Footprints (blue).

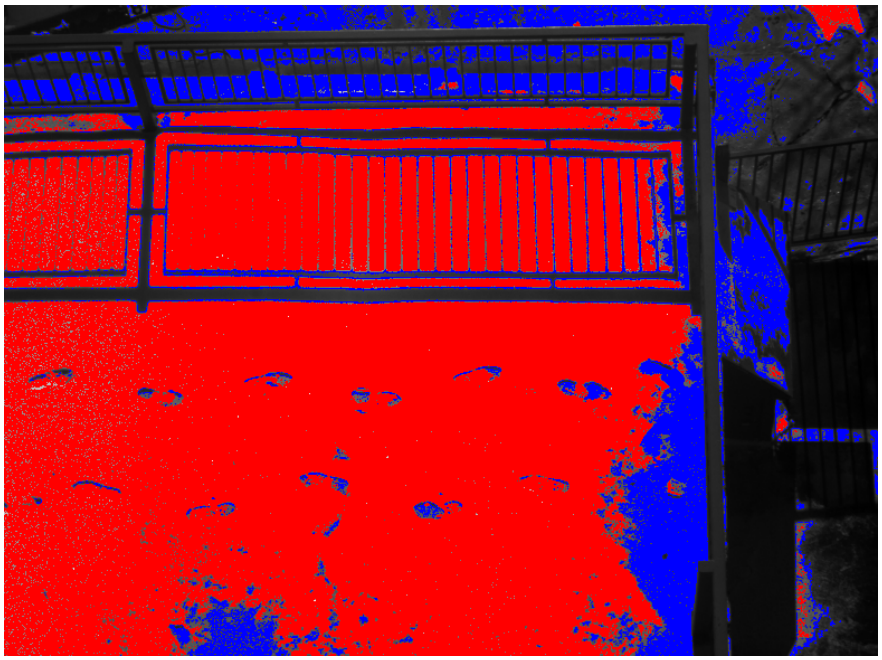

Figure 27. Intensity Image (S0) with ROI Overlay: Background (red) and footprints (blue).

The IDL programming software then generated two normalized histograms comparing the occurrences of DOLP for both the background and disturbed snow and the occurrences of inverse intensity for the same regions. Figures 28 and 29 show that the separation of peaks between the regions of interest in terms of standard deviations were greater for the inverse intensity plot (3.7σ) than the DOLP plot (1.3σ) where the difference was approximately 2.4σ. This indicates that intensity is stronger than polarization in detecting disturbances for this image.

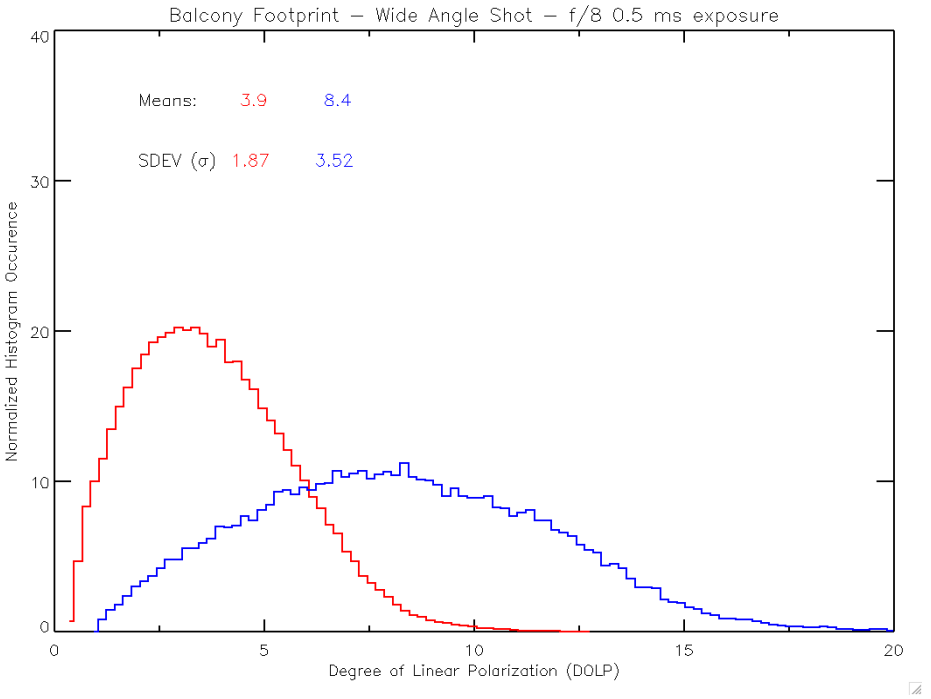

Figure 28. Normalized Histogram of DOLP Occurrences for the Wide-Angle Balcony Image: Background (red) and Footprints (blue).

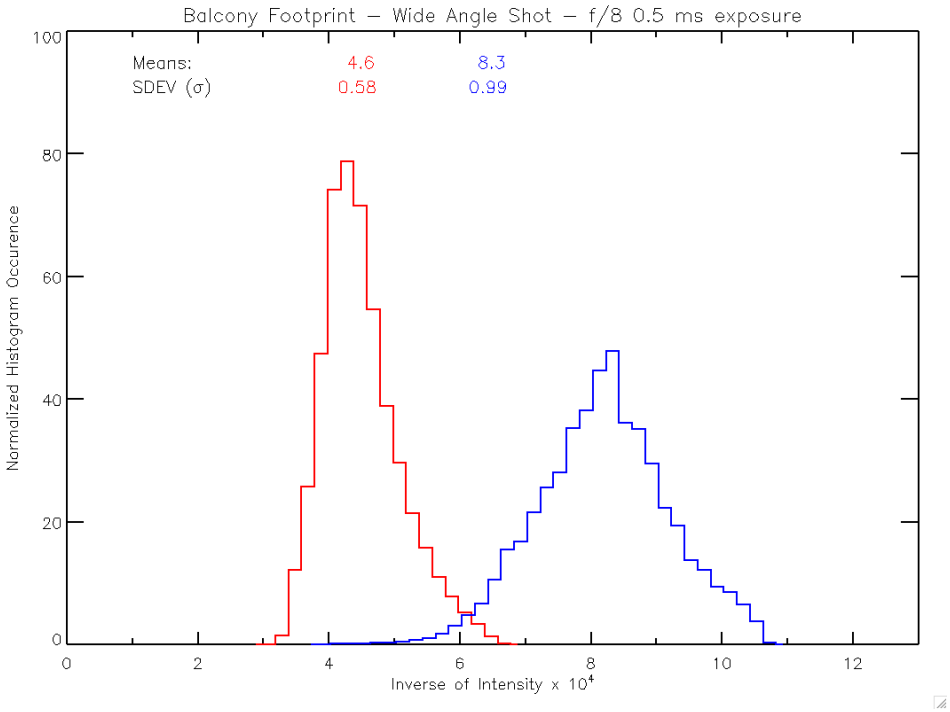

Figure 29. Normalized Histogram of Intensity Occurrences for the Wide-Angle Balcony Image: Background (red) and Footprints (blue).

2. Telephoto Lens Image

The next image is from the same balcony scene as the previous image, but a telephoto zoom lens was used to isolate a single footprint. Note that the texture of the footprint in Figure 30(a) indicates that there is snow and not concrete appearing in the image. Figure 30(b) shows the corresponding DOLP calculation, which indicates that there is a significant change in polarization as the image moves from disturbed to undisturbed snow. Figure 31 shows the five texture images produced by ENVI where the ASM and Entropy algorithms were the best methods for isolating the polarized footprint.

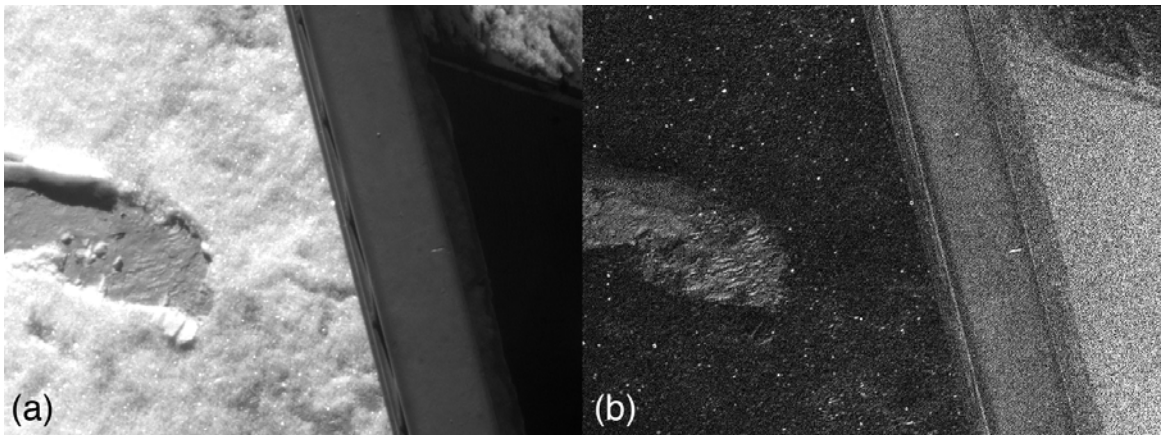

Figure 30. Zoomed Image of Disturbed Snow from 7th Story Balcony: (a) Intensity and (b) DOLP.

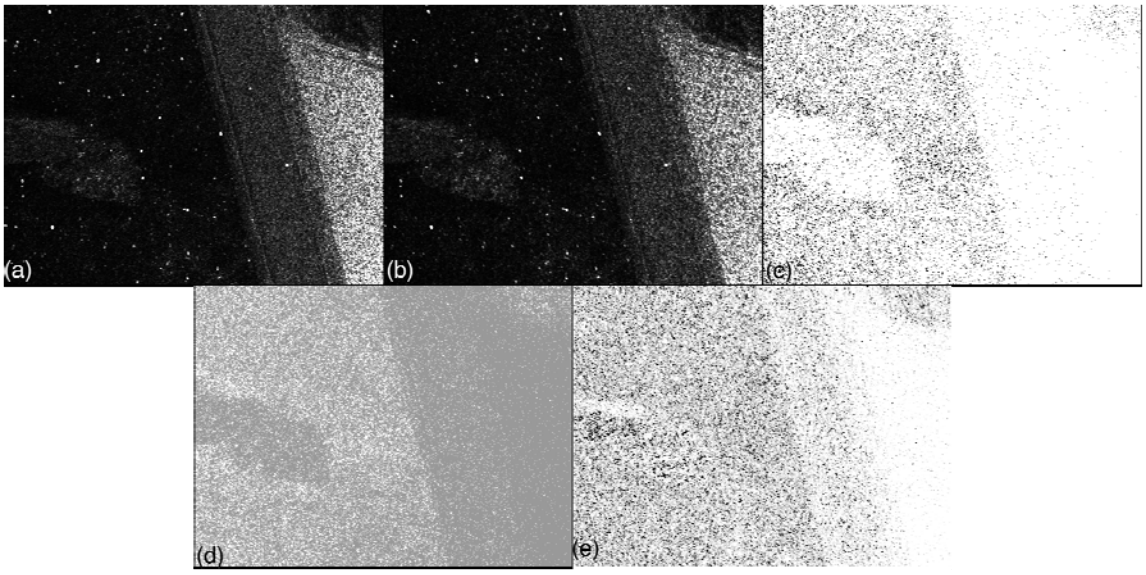

Figure 31. Texture Filters Applied to Zoomed Image from 7th Story Balcony: Variance (a), Contrast (b), Entropy (c), ASM (d), and Correlation (e).

Just as in the wide-angle image, a scatter plot of DOLP versus inverse intensity was created in ENVI to isolate the disturbed and undisturbed snow. ROIs were established and then plotted in Figures 32, 33, and 34. These figures show that there were detectable and isolatable differences in polarization and intensity between the disturbed and undisturbed snow. While the scale of these plots indicates that the differences are minor, they also show that the differences are nonnegligible.

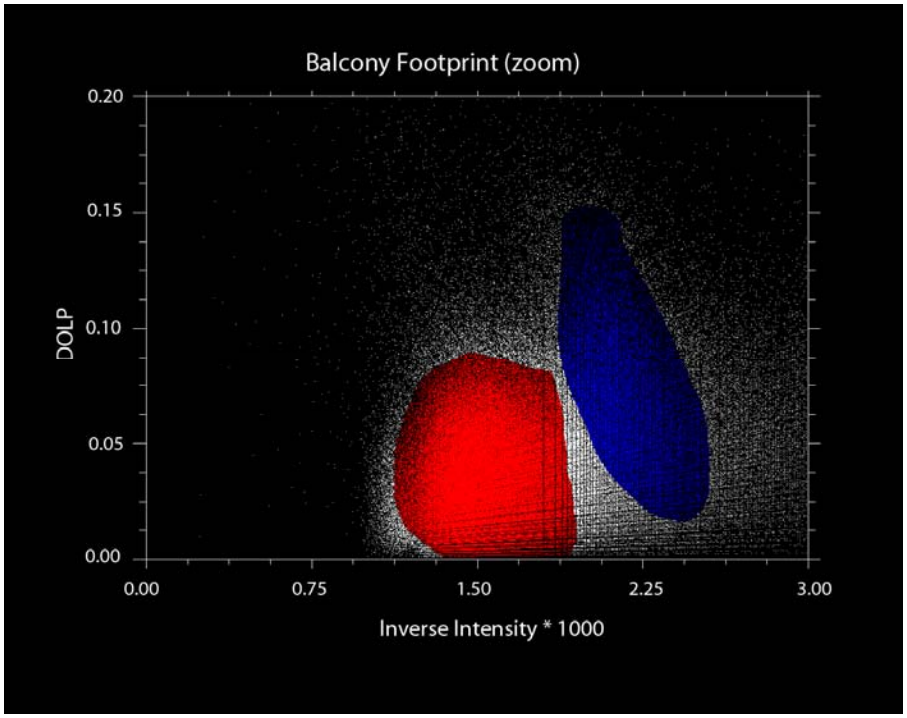

Figure 32. Cropped Scatter Plot of Regions of Interest for the Zoomed Balcony Image: Background (red) and Footprints (blue).

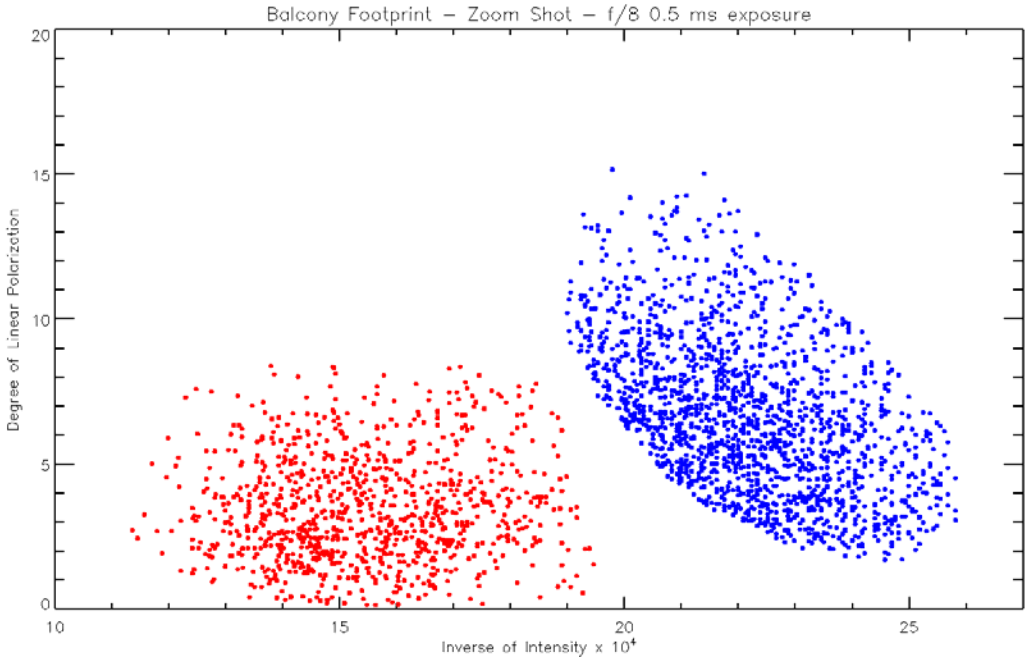

Figure 33. Simplified Scatter Plot of Regions of Interest for the Zoomed Balcony Image: Background (red) and Footprints (blue).

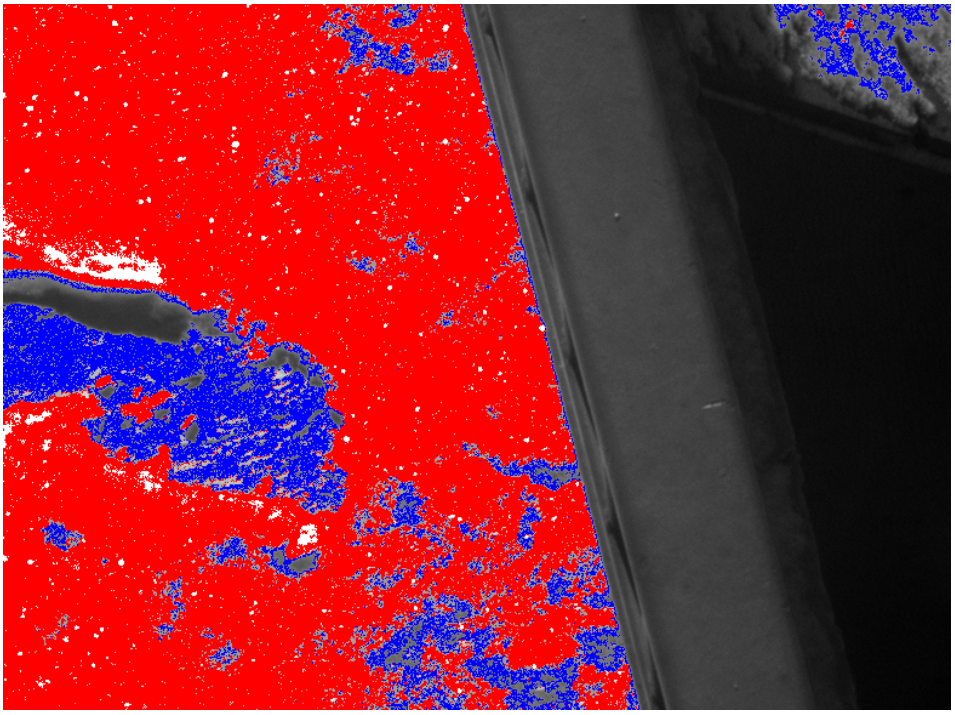

Figure 34. Intensity Image (S0) with ROI Overlay: Background (red) and footprints (blue).

Again, IDL was used to create the histograms of DOLP and inverse intensity for the two regions of interest designated on the scatter plot. Figures 35 and 36 show the separation of peaks in the DOLP histogram was approximately 1.2σ and the separation of peaks in the inverse intensity histogram was 4.1σ. This gave an overall difference in peak separation of 2.9σ, which was greater than the 2.4σ value given by the wide-angle image.

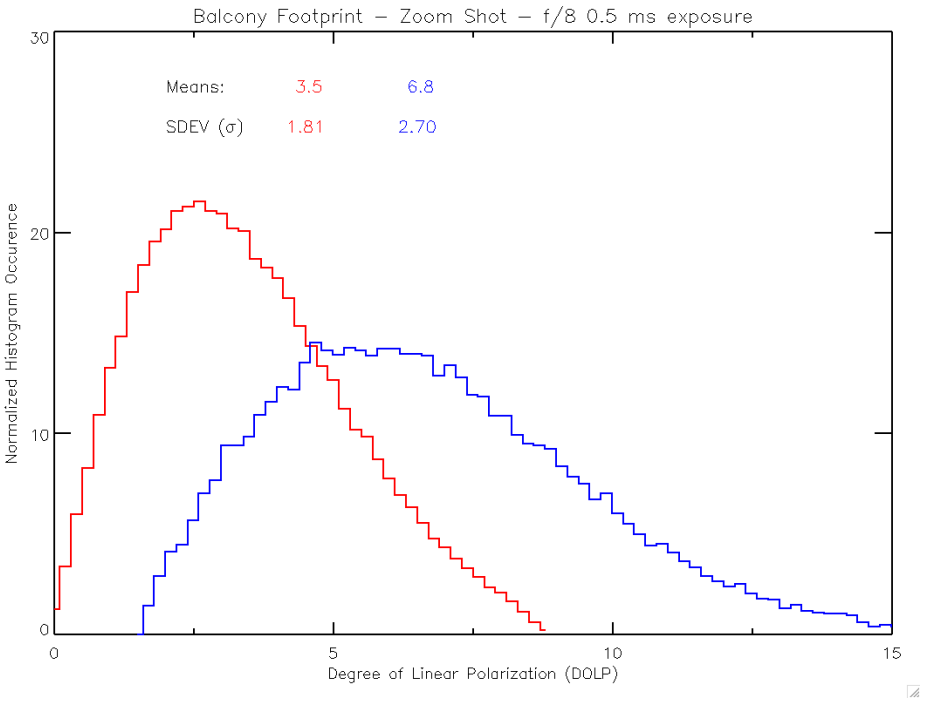

Figure 35. Normalized Histogram of DOLP Occurrences for the Zoomed Balcony Image: Background (red) and Footprints (blue).

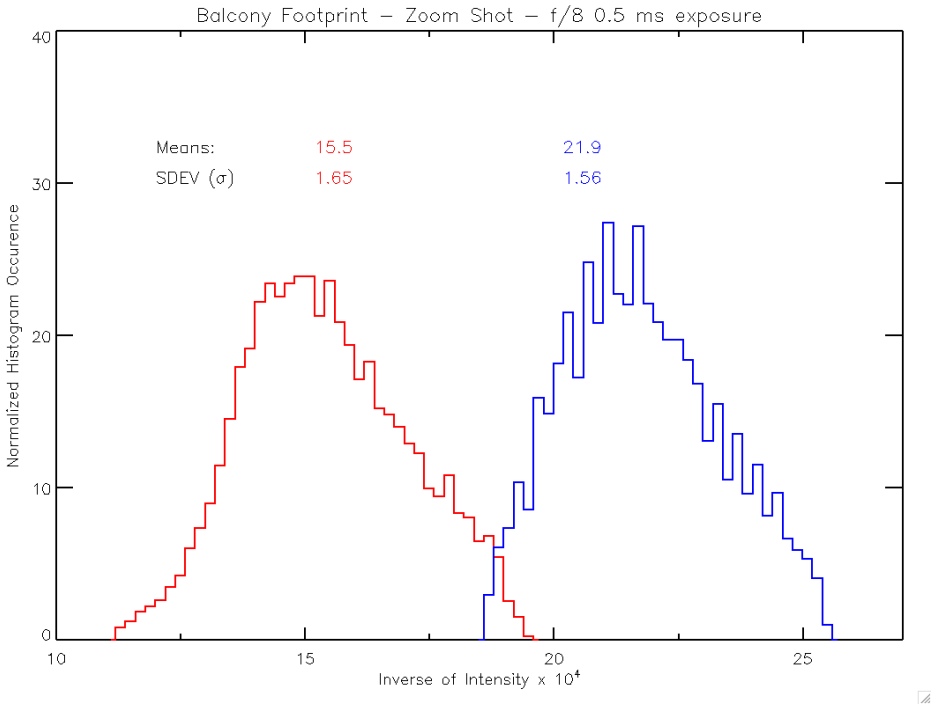

Figure 36. Normalized Histogram of Intensity Occurrences for the Zoomed Balcony Image: Background (red) and Footprints (blue).

B. GOLF COURSE (PARK)

1. Close-Up of Footprint - 180 Degrees From Sun

The footprint in the park was substantially different than the one imaged from the 7th-story balcony using a telephoto lens. This footprint was created in deep snow that was much drier and left an imprint approximately 2 inches deep. It was photographed at close to 180 degrees with respect to the sun, as this was believed to be the angle at which polarization would be at an observable maximum. Figure 37 compares the original intensity image of the footprint and ENVI's calculated DOLP image, which shows polarization data allows the naked eye to detect the disturbance, just not as well as using the intensity data. Figure 38 is a combination of texture filters applied to the DOLP calculation and provides the eye with a moderate amount of enhancement to the footprint.

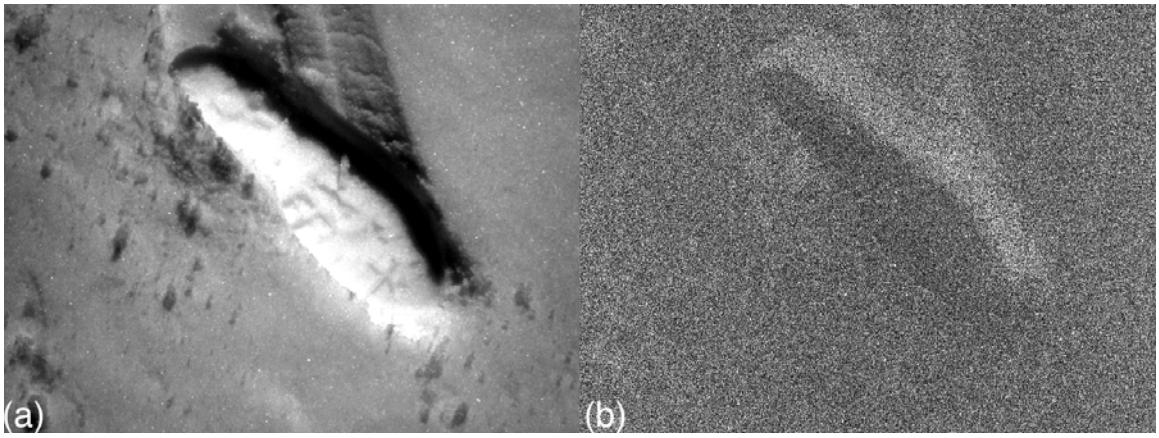

Figure 37. Close-Up of Park Footprint at 180 Degrees From Sun: (a) Intensity and (b) DOLP.

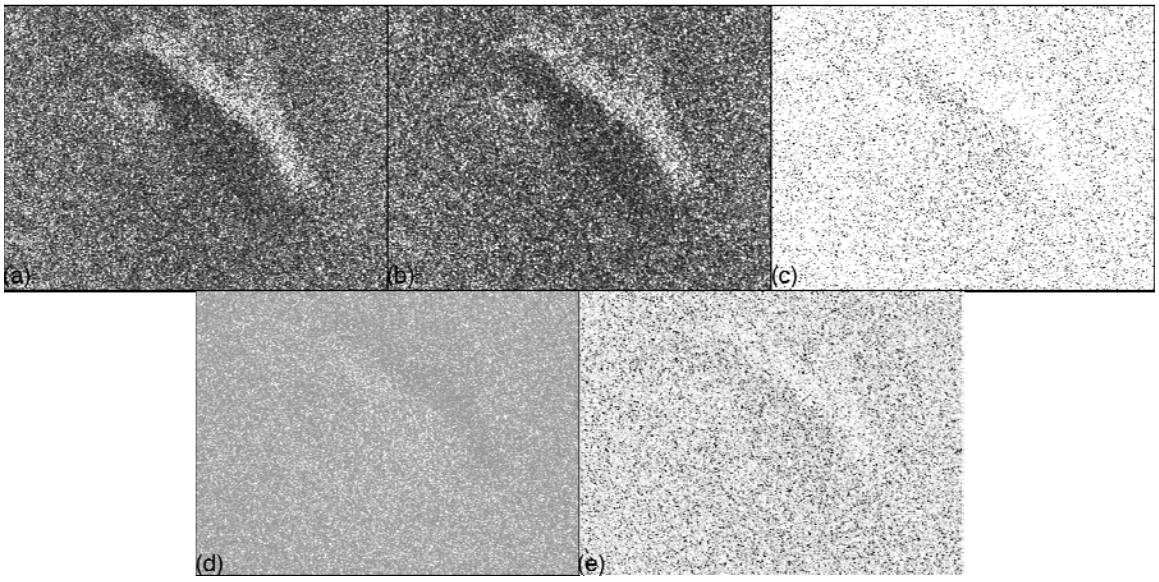

Figure 38. Texture Filters Applied to Close-Up Park Footprint at 180 Degrees From Sun: Variance (a), Contrast (b), Entropy (c), ASM (d), and Correlation (e).

After creating a two-dimensional scatter plot, regions of interest were selected to isolate the footprint from the background snow that can be seen in Figure 35. This scatter plot corresponds with the intensity image of Figure 39(a) where the footprint (blue) is brighter than that of the background (red). Note in the figure how there is little difference in polarization between the footprint and the background snow. This indicates that using polarization to detect the footprint is not as useful as intensity. The histograms from the ROI of DOLP and intensity are shown in Figures 40 and 41 and again show that the footprint's polarization is slightly less that the background. This corresponds to the Umov effect discussed earlier. Also note that the histograms show the separation between peaks is 0.4σ for DOLP and is 4.0σ for intensity. The difference in peak separation is 3.6σ indicating that the intensity image still allows for better differentiation between disturbed and undisturbed snow.

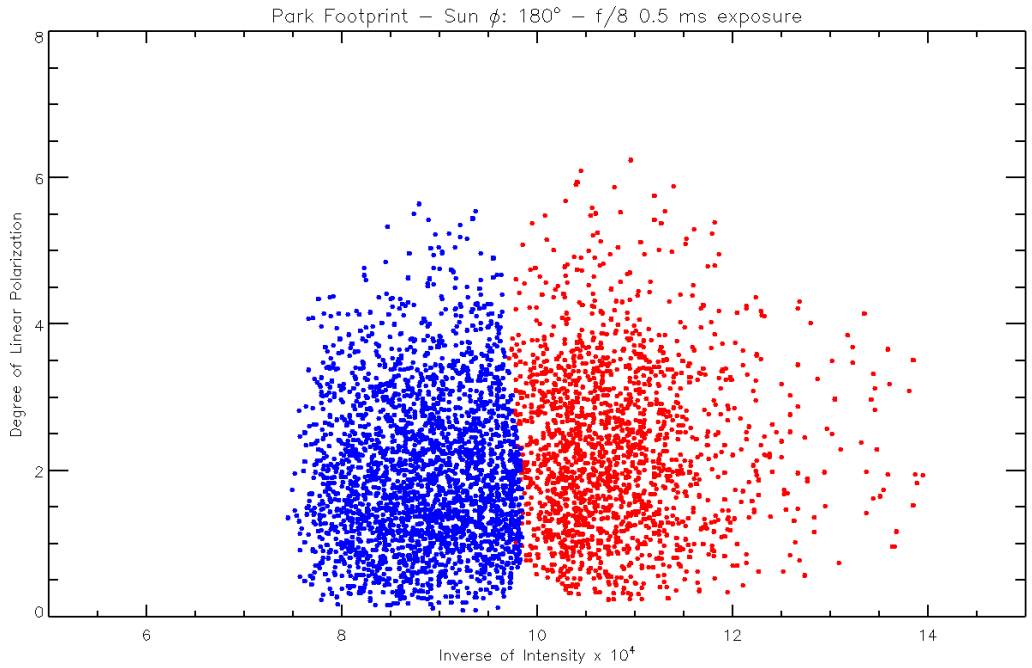

Figure 39. Simplified Scatter Plot of Regions of Interest for Close-up Park Footprint at 180 Degrees From Sun: Background (red) and Footprints (blue).

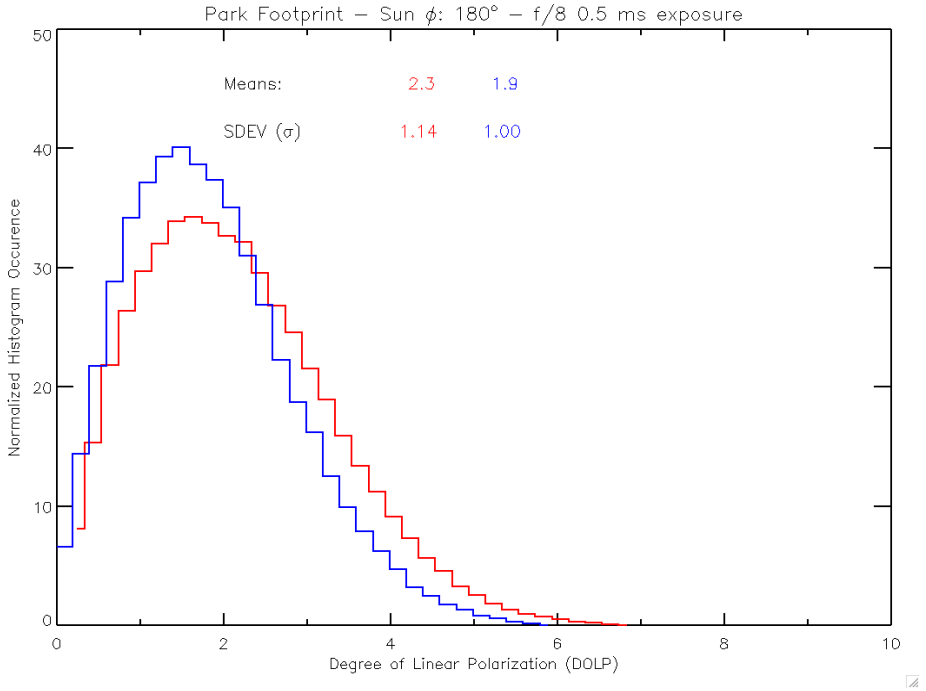

Figure 40. Normalized Histogram of DOLP Occurrences for Close-up Park Footprint Image at 180 Degrees From Sun: Background (red) and Footprints (blue).

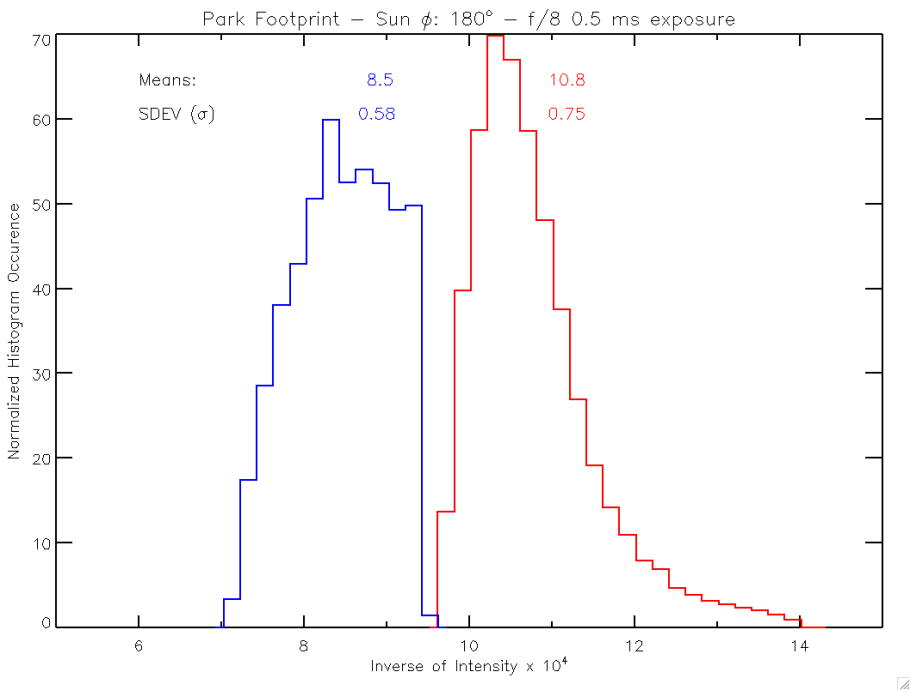

Figure 41. Normalized Histogram of Intensity Occurrences for Close-up Park Footprint Image at 180 Degrees From Sun: Background (red) and Footprints (blue).

2. Close-Up of Footprint—0, 90, and 270 Degrees From Sun

The same footprint was also imaged from the three other primary directions with respect to the sun to determine if the orientation of observation changed the amount of polarization received by the camera. Figures 42 through 47 show the histograms for both DOLP and intensity for 0-, 90-, and 270-degree orientations. These figures show very little differentiation from the image taken at 180 degrees from the sun. Appendix A summarizes the differences in peak separation for all four observation directions.

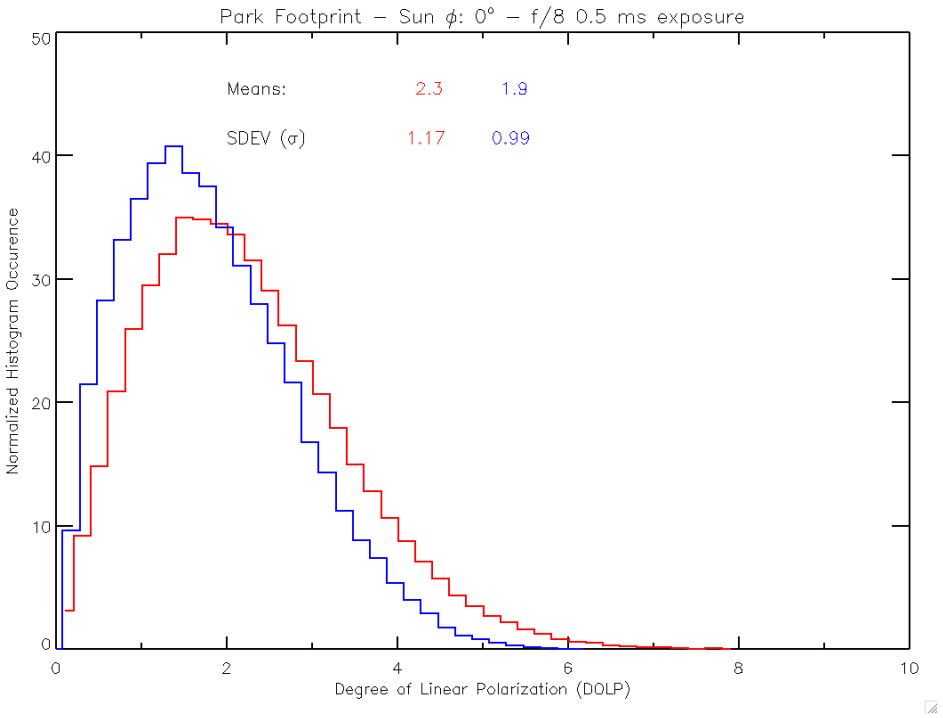

Figure 42. Normalized Histogram of DOLP Occurrences for Close-up Park Footprint Image at 0 Degrees From Sun: Background (red) and Footprints (blue).

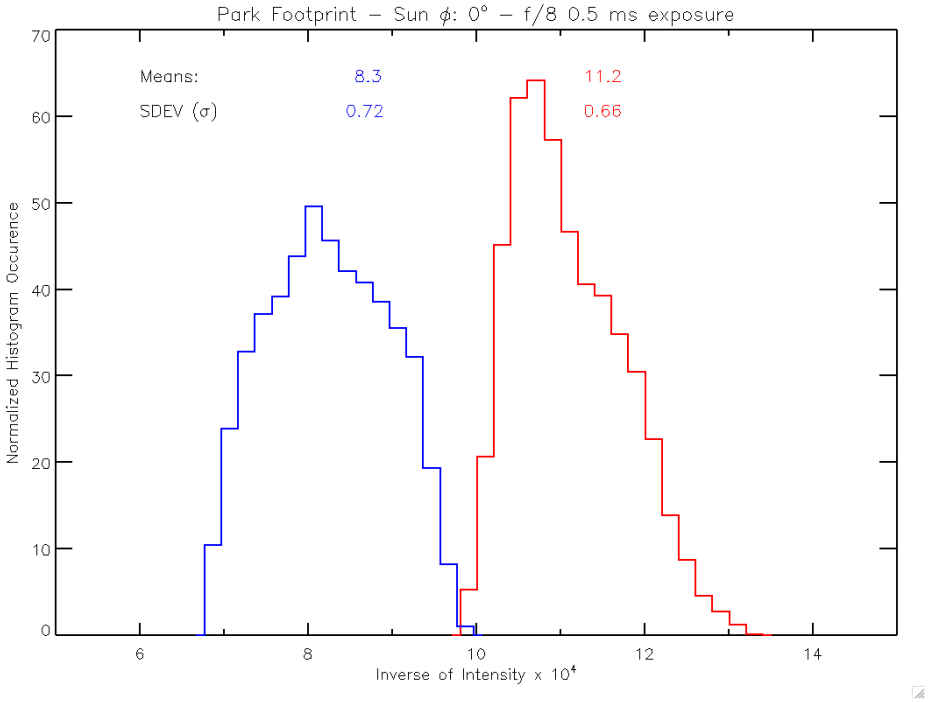

Figure 43. Normalized Histogram of Intensity Occurrences for Close-up Park Footprint Image at 0 Degrees From Sun: Background (red) and Footprints (blue).

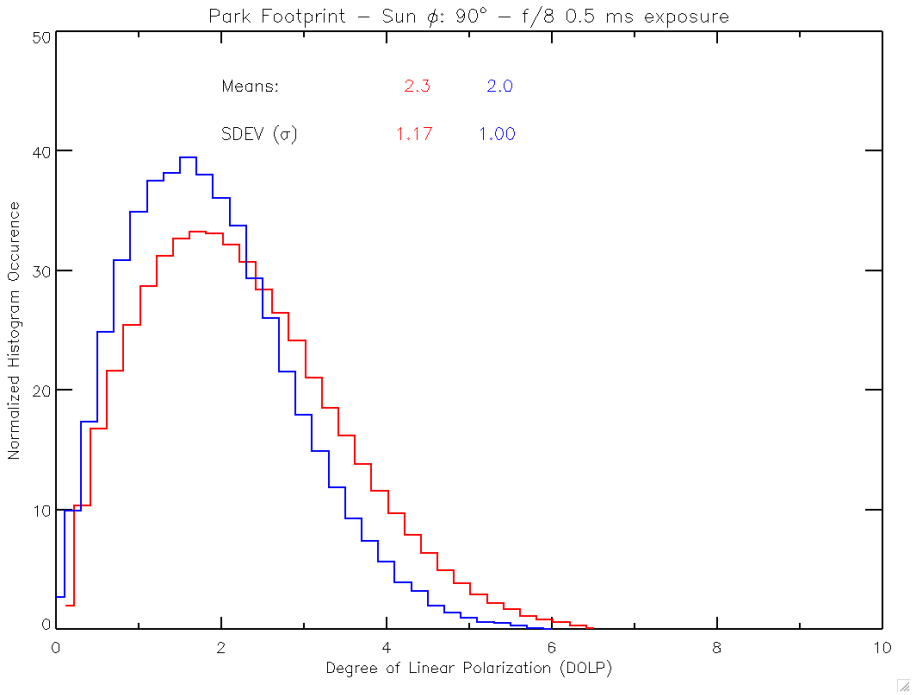

Figure 44. Normalized Histogram of DOLP Occurrences for Close-up Park Footprint Image at 90 Degrees From Sun: Background (red) and Footprints (blue).

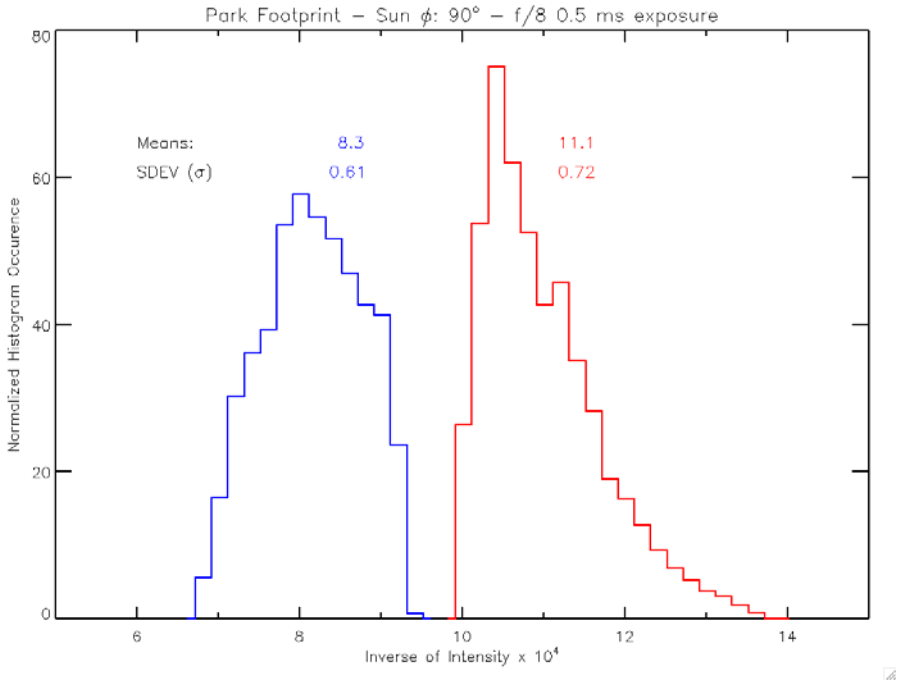

Figure 45. Normalized Histogram of Intensity Occurrences for Close-up Park Footprint Image at 90 Degrees From Sun: Background (red) and Footprints (blue).

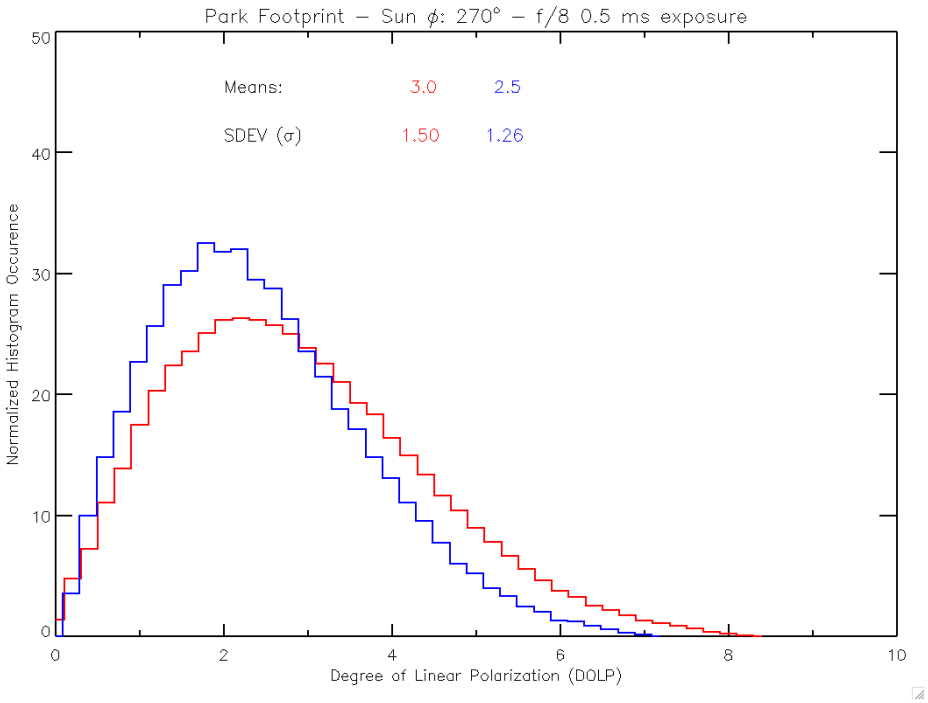

Figure 46. Normalized Histogram of DOLP Occurrences for Close-up Park Footprint Image at 270 Degrees From Sun: Background (red) and Footprints (blue).

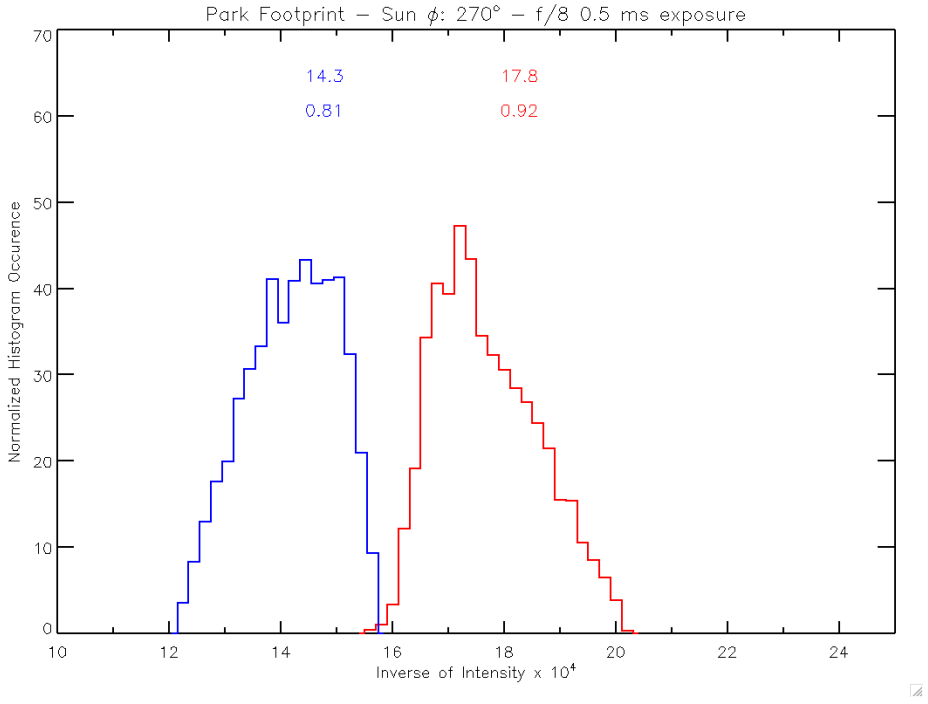

Figure 47. Normalized Histogram of Intensity Occurrences for Close-up Park Footprint Image at 270 Degrees From Sun: Background (red) and Footprints (blue).

3. Snowmobile Tracks

The final image was also taken at the Tahoe City Golf Course and consisted of recently made snowmobile tracks in fresh snow. Figure 48 shows a side-by-side comparison of the intensity image to that of the DOLP image calculated by ENVI. This figure shows again that there was not much polarization within the snowmobile tracks when compared to the other objects in the image, such as the building shadows and the polarizing filter being held by the research assistant. Figure 49 shows the application of the texture filter algorithms to the DOLP data and again, the ASM and entropy algorithms worked best at isolating the disturbance for the naked eye.

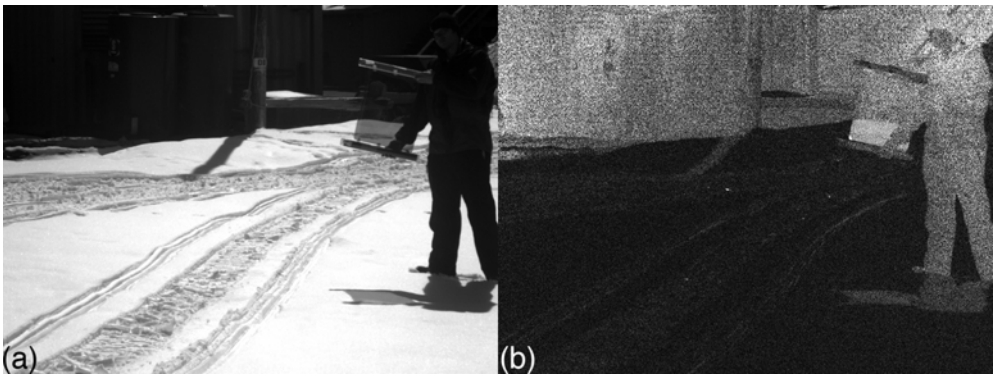

Figure 48. Snowmobile Tracks at 180 Degrees From Sun: (a) Intensity and (b) DOLP.

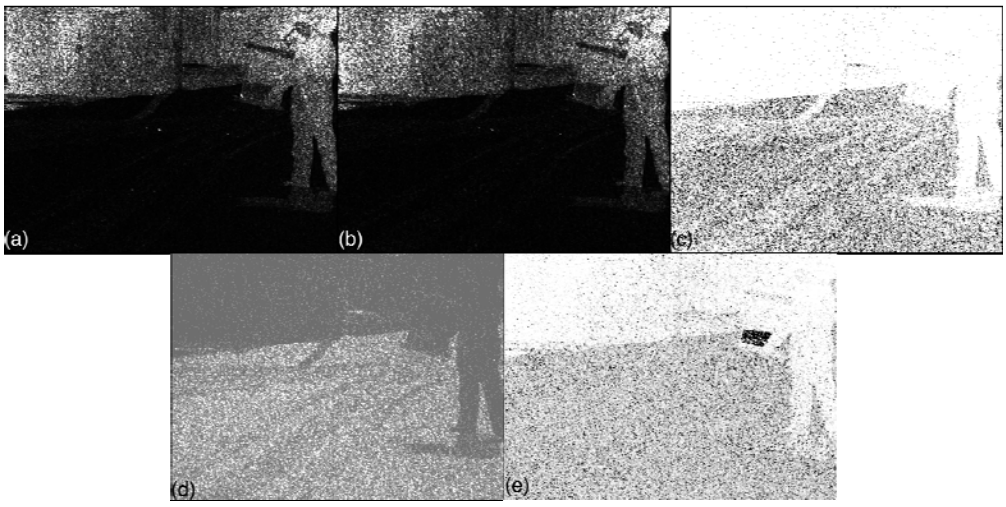

Figure 49. Texture Filters Applied to Snowmobile Tracks at 180 Degrees From Sun: Variance (a), Contrast (b), Entropy (c), ASM (d), and Correlation (e).

Figure 50 shows the scatter plot for the disturbed snow (red) and the snowmobile tracks (blue) and Figure 51 shows the ROI overlay of the image, which indicates the separability of the disturbance from the background. There are two interesting things to note with these figures. The first is that the difference in intensity between the two snow types was greater than any of the previous images. The second is that the polarization filter in the scene (shown in green) causes approximately 50% polarization in the incident light. Figures 52 and 53 are the IDL histogram plots of the DOLP and inverse intensity ROIs, which shows the peak separation for DOLP was, 0.85σ and 2.8σ for inverse intensity. This gave a difference in peak separations of 1.95σ, the smallest of the analyzed images.

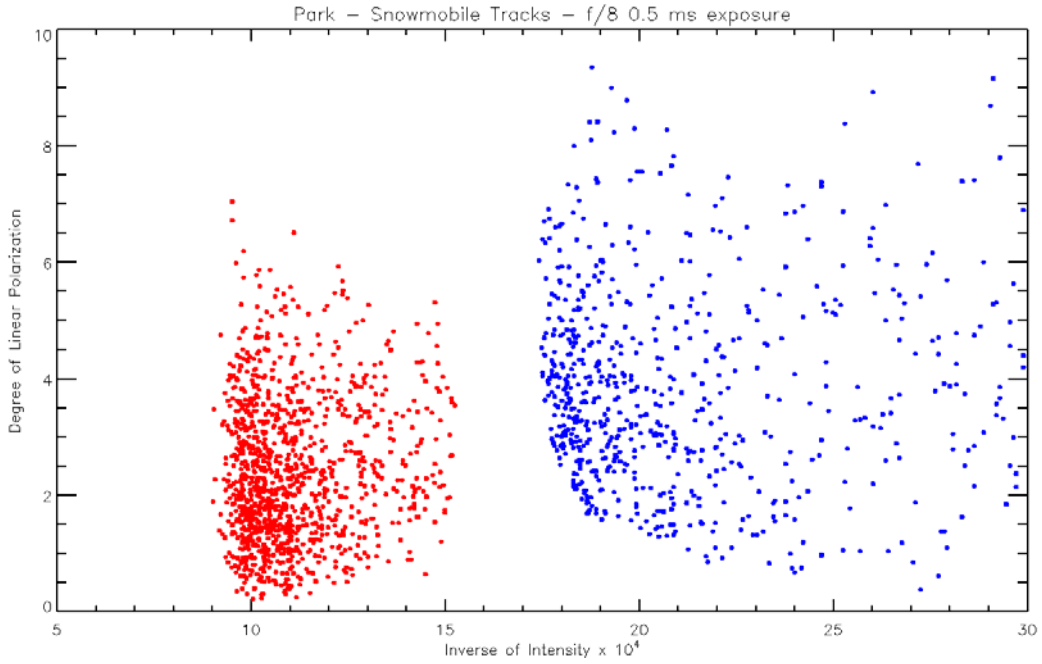

Figure 50. Simplified Scatter Plot of Regions of Interest for Snowmobile Tracks at 180 Degrees From Sun: Background (red) and Footprints (blue).

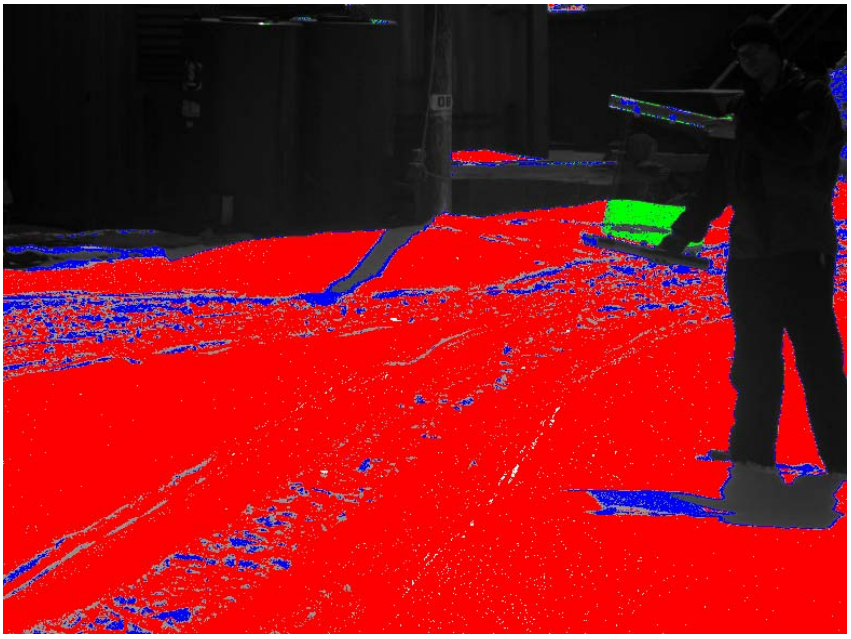

Figure 51. Intensity Image (S0) with ROI Overlay: Background (red) and footprints (blue).

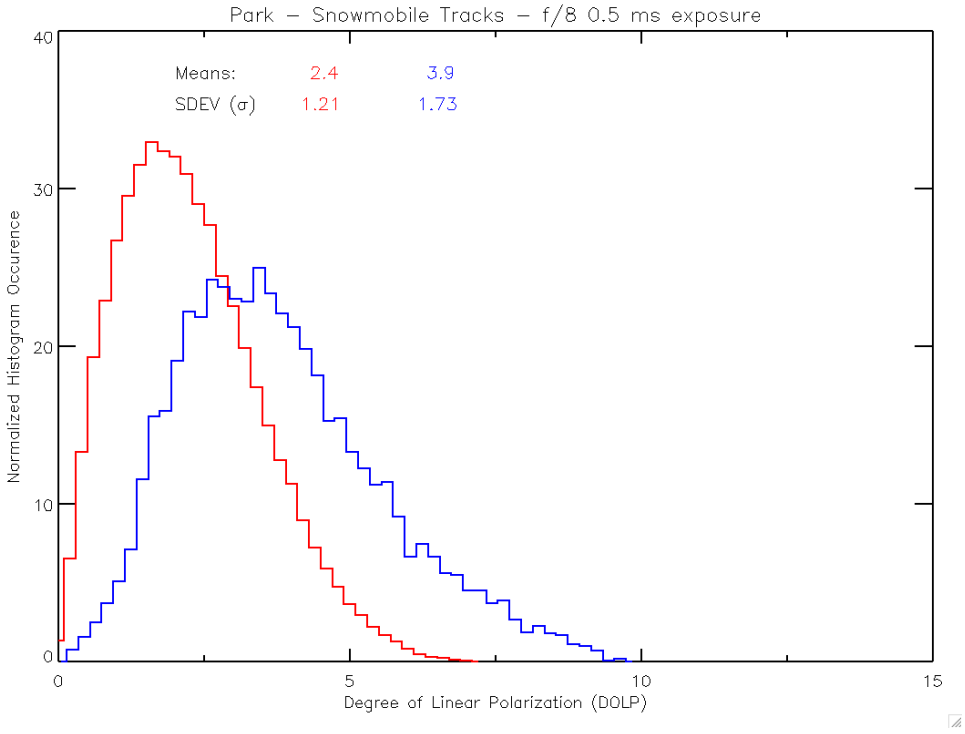

Figure 52. Normalized Histogram of DOLP Occurrences for Snowmobile Tracks at 180 Degrees From Sun: Background (red) and Footprints (blue).

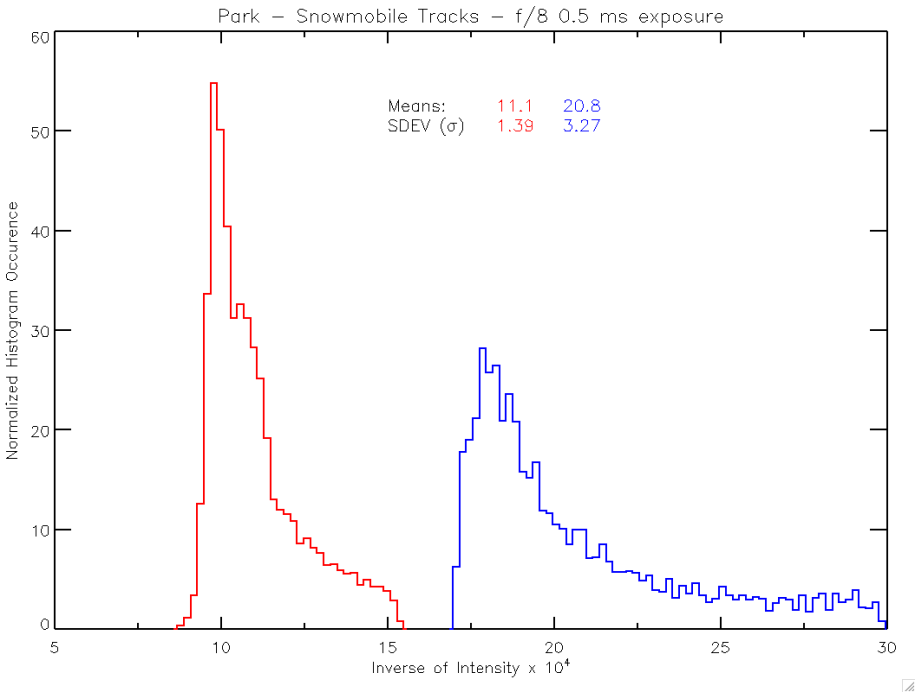

Figure 53. Normalized Histogram of Intensity Occurrences for Snowmobile Tracks at 180 Degrees From Sun: Background (red) and Footprints (blue).

The snowmobile track image was also used to validate the camera's polarization functionality and to see if the Umov Effect was occurring as predicted. ENVI created a scatter plot of DOLP versus intensity and then a scatter plot of DOLP versus inverse intensity. A density slice algorithm was applied to the scatter plot, which assigned colors to groupings of data points where red is the densest and blue the least. Figure 54 is the density slice of DOLP versus intensity and shows the very bright snow having very little polarization. Note the bright spot indicating the filter that polarizes the incident light by approximately 50%. Figure 55 is the density slice of DOLP versus inverse intensity and shows a linear x-y correlation between dark objects and higher degrees of polarization. These figures confirm two important principles. The first is that snowy scenes are typically bight and have low amounts of polarization. The second is that the Umov Effect holds true for images containing primarily snow.

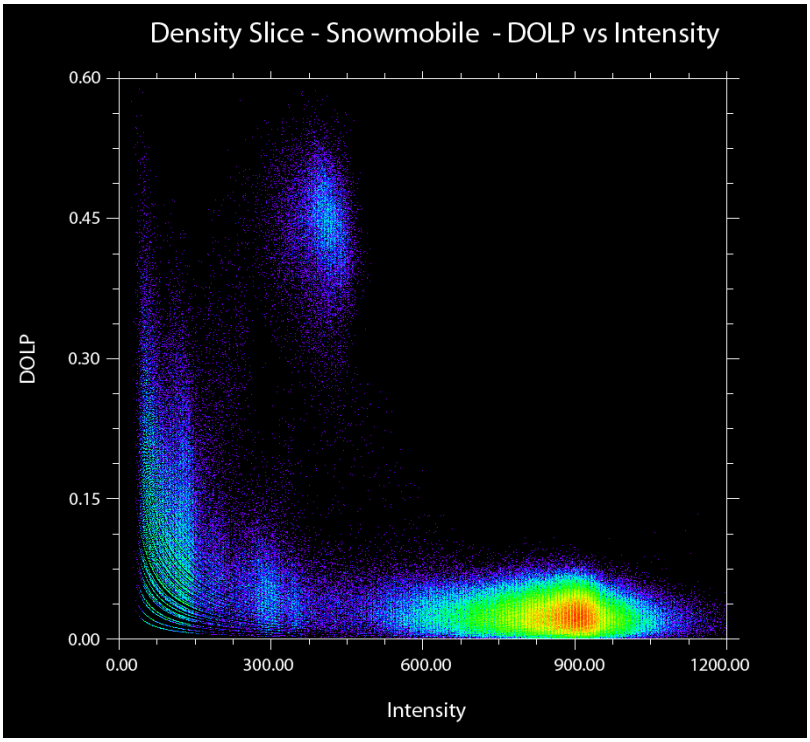

Figure 54. DOLP Versus Intensity for Snowmobile Tracks at 180 Degrees from Sun

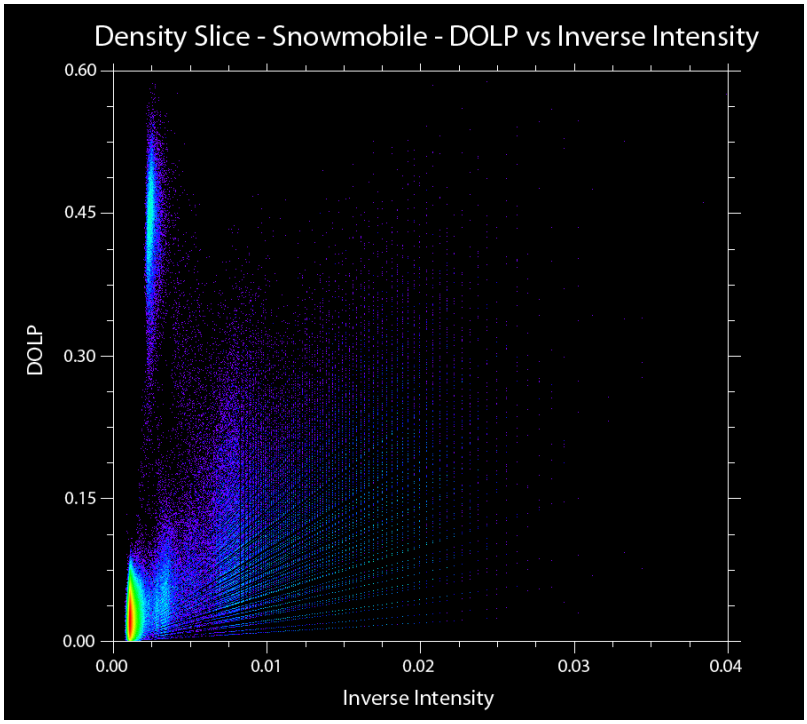

Figure 55. DOLP Versus Inverse Intensity for Snowmobile Tracks at 180 Degrees from Sun

V. CONCLUSION

A. SUMMARY OF OBSERVATIONS AND ANALYSIS

The SALSA polarimetric camera from Bossa Nova Technologies was used to image disturbed and nondisturbed snow to determine if a significant and detectable change in polarization occurred to reflected light. Images of footprints in both deep and shallow snow depths, as well as snowmobile tracks, were captured and analyzed by computer algorithms to enhance the detection of polarization changes. These algorithms consisted of Haralick occurrence texture filters, scatter plots with regions of interest, and normalized histograms.

The primary result of this research was that polarization changes were minor compared to the changes of intensity between disturbed and nondisturbed snow. This was shown by the histograms for intensity and DOLP where the separation of peaks for DOLP was much smaller, and thus less detectable, than for intensity. However, while polarization may not be as useful as intensity, the measurement provided a detectable and meaningful signature.

The texture filters applied to the DOLP images enhanced detection for the naked eye but did not increase the observer's ability to detect disturbances when compared to the intensity image. This was most likely due to the low amounts of polarization being produced by the snow, which was predicted by the Umov Effect.

Overall, polarization changes between disturbed and nondisturbed snow is measurable but small. While not insignificant, it is not as effective as using intensity data to detect disturbances. Additionally, the results of this research showed that the SALSA camera was performing correctly and adequately captured polarization data within snowy images.

B. RECOMMENDATIONS AND FUTURE WORK

The research conducted for this thesis did not have elevation controls for the camera. If the camera could be positioned closer to the Brewster's Angle, more polarization information may be captured and provide a stronger data set which could detect the disturbances better than intensity. In regards to the shallow snow footsteps seen from the balcony of the hotel, subsurface objects may cause greater changes to polarization as light is reflected off the object and back out of the snow surface. Further study should be conducted in this area.

Additionally, it is recommended that the camera or similar polarimetric sensors be used on airborne platforms to provide an image similar to those needed by intelligence analysts. These images could than be compared to the results of this research to see if there are significant changes to the peak separations for DOLP and intensity when there are greater distances between the sensor and the object.

APPENDIX A

Table 2. Summary of Peak Separation for Images Analyzed by ENVI and IDL. Units are in Terms of Standard Deviation.

Image	DOLP Peak Separation	Intensity Peak Separation	Difference
7th Floor Balcony - Wide	1.3	3.7	2.4
7th Floor Balcony - Zoom	1.2	4.1	2.9
Park Footprint - 0 Degrees	0.4	4.0	3.6
Park Footprint - 90 Degrees	0.3	4.6	4.3
Park Footprint - 180 Degrees	0.4	4.0	3.6
Park Footprint - 270 Degrees	0.4	4.3	3.9
Snowmobile Tracks	0.9	2.8	1.9

THIS PAGE INTENTIONALLY LEFT BLANK

APPENDIX B

```
; Code used to produce histograms and scatterplots for thesis:
;   Disturbance Detection In Snow Using Polarimetric Imagery of the
;   Visible Spectrum
; Written by Professor R.C. Olsen, 08NOV2010
; Modified by Lieutenant Commander David West, 15NOV2010

;*****************************************************************
;File Setup

; Select colors for graphs
red = 255L
green = 256* red
blue = 256 * green
white = red + blue + green
black = 0

; Establish user directory where images are located
dir = '/Users/DaveWest/Desktop/Image Analysis'

; Name files for saving generated charts
cd, dir
roi_file = 'ImageROIData.txt'
scatter_plot_file = 'Image_Scatter_Plot_Balcony_F8_half_ms_WideAngle'
Dolp_hist_file   = 'Image_DOLP_Hist_Balcony_F8_half_ms_WideAngle'
II_hist_file =    'Image_II_Hist_Balcony_F8_half_ms_WideAngle'

;*****************************************************************
; Read in data from Region of Interest File (generated by ENVI)

openr, 1, roi_file
hdr = ' '
for i = 0, 3 do begin
readf, 1, hdr
print, hdr
endfor
print, 'first region'
for i = 1, 3 do begin
readf, 1, hdr
print, hdr
endfor
nlen = strlen(hdr)
offset = 12
delta = nlen - offset
str = strmid( hdr, offset, delta)
help, str & print, str
n1 = long(str)   & help, n1
region1 = fltarr( 2, n1)

readf, 1, hdr
print, hdr
print, 'second region'
```

```
for i = 1, 3 do begin
readf, 1, hdr
print, hdr
endfor
nlen = strlen(hdr)
offset = 12
delta = nlen - offset
str = strmid( hdr, offset, delta)
help, str & print, str
n2 = long(str)  & help, n2
region2 = fltarr( 2, n2)

readf, 1, hdr
print, hdr

ii = intarr(3) & data = fltarr(2)
for i = 0L, n1-1 do begin
readf, 1, ii, data
;print, ii, data
region1(*,i) = data(*)
endfor
window, 1
x = 1e4*region1(1,*)  & y = 100*region1(0,*)
;  stats for region 1
stats_region1_II = moment(x, sdev = sdev_region1_II)
stats_region1_DOLP = moment (y, sdev = sdev_region1_DOLP)
mean_region1_II   = stats_region1_II(0)
mean_region1_DOLP = stats_region1_DOLP(0)

erase, white
radius = 1
circle = 2*!pi*findgen(9)/8
usersym, radius* cos(circle), radius*sin(circle), /fill

dolp_hist_factor = 5.0
intens_hist_factor = 5.0

;*******************************************************************
;Create plot parameters (title, ranges, etc...)

!p.title = 'Balcony Footprint - Wide Angle Shot - f/8 0.5 ms exposure'

plot, x, y, psym = 3, xrange = [0, 13], yrange = [0, 20], $
  color = 0, /noerase, /nodata, xthick = 2, ythick = 2, xstyle = 1, $
  xtitle = 'Inverse of Intensity x 10!u4!n', ytitle = 'Degree of Linear
Polarization', $
  charsize = 1.8
  red_factor = 200L
red_index = red_factor*findgen( n1/float(red_factor))
oplot, x(red_index), y(red_index), psym = 8, color = red

;*******************************************************************
; Create Scatter Plot

h1_red = histogram( intens_hist_factor*x, omin = min_r1, omax = max_r1)
```

```
n1_red = n_elements( h1_red)
x1_red = [findgen(n1_red+2) + min_r1-1 ]/intens_hist_factor
h1_red = h1_red*intens_hist_factor
h1_red = [ 0, h1_red, 0] & help, h1_red, x1_red

h2_red = histogram( dolp_hist_factor*y, omin = min_r2, omax = max_r2)
n2_red = n_elements( h2_red)
x2_red = [findgen(n2_red) + min_r2] /dolp_hist_factor
h2_red = h2_red*dolp_hist_factor

wshow

readf, 1, hdr
print, hdr
ii = intarr(3) & data = fltarr(2)
for i = 0L, n2-1 do begin
readf, 1, ii, data

region2(*,i) = data(*)
endfor

x = 1e4*region2(1,*)  & y = 100*region2(0,*)
stats_region2_II = moment(x, sdev = sdev_region2_II)
stats_region2_DOLP = moment (y, sdev = sdev_region2_DOLP)
print, 'stats_region2_DOLP'
print, stats_region2_DOLP
mean_region2_II = stats_region2_II(0)
mean_region2_DOLP = stats_region2_DOLP(0)

blue_factor = 20.
blue_index = blue_factor*findgen( n1/blue_factor)
oplot, x(blue_index)+0.3, y(blue_index), psym = 8, color = blue
h1_blue = histogram( intens_hist_factor*x, omin = min_g1, omax =
max_g1)
n1_blue = n_elements( h1_blue)
x1_blue = [findgen(n1_blue+2) + min_g1 -1]/intens_hist_factor
h1_blue = [ 0, h1_blue, 0] & help, h1_blue
h1_blue = h1_blue *intens_hist_factor

h2_blue = histogram( dolp_hist_factor*y, omin = min_g2, omax = max_g2)
n2_blue = n_elements( h2_blue)
x2_blue = [findgen(n2_blue+2) + min_g2 - 1  ]/dolp_hist_factor
h2_blue = [ 0, h2_blue, 0] & help, h2_blue
h2_blue = h2_blue * dolp_hist_factor

; Write Scatter Plot to File
im = tvrd(true = 1)
write_tiff, scatter_plot_file + '.tif',   reverse(im,3)
write_jpeg, scatter_plot_file + '.jpg', im, true = 1, quality = 98

;*****************************************************************
; Create Inverse of Intensity Histogram

window, 2, xsize = 1100, ysize = 800
erase, white
```

```
 !x.thick = 2 & !y.thick = 2
 !p.charsize = 2
   !y.title = 'Normalized Histogram Occurence'

plot, x1_red,  h1_red*100./n1, /noerase, color = 0, /nodata, $
 yrange = [0, 100], ystyle = 1, xstyle = 1, $
 xrange = [0, 13], xtitle = 'Inverse of Intensity x 10!u4!n', $
 charsize = 1.8, yminor = 1, xminor = 2
oplot, x1_red+0.03,  h1_red*100./n1, color = red, psym = 10, thick = 2
oplot, x1_blue, h1_blue*100./n2, color = blue, psym = 10, thick = 2
xx1 = mean_region1_II
xx2 = mean_region2_II
yyii = 94
yyjj = 90
xyouts, 1, yyii, 'Means: ', color = black
xyouts, 1, yyjj, 'SDEV (!4r!3)', color = black
xx1 = 4
xx2 = 6
xyouts, xx1, yyii, string(mean_region1_II, format ="(F5.1)"), color =
red
xyouts, xx1, yyjj, string(sdev_region1_II, format ="(F5.2)"), color =
red
xyouts, xx2, yyii, string(mean_region2_II, format ="(F5.1)"), color =
blue
xyouts, xx2, yyjj, string(sdev_region2_II, format ="(F5.2)"), color =
blue

; Write Inverse of Intensity Plot to File
im = tvrd(true = 1)
write_tiff, II_hist_file + '.tif',   reverse(im,3)
write_jpeg, II_hist_file + '.jpg', im, true = 1, quality = 98

;*******************************************************************
;Create DOLP Histogram

window, 0, xsize = 1100, ysize = 800
erase, white
plot, x2_red,  h2_red*100./n1, /noerase, color = 0, /nodata, $
 xrange = [0, 16], yrange = [0, 35], xtitle = 'Degree of Linear
Polarization (DOLP)', $
 charsize = 1.8, yminor = 1, xminor = 2
oplot, x2_red,  h2_red*100./n1, color = red, psym = 10, thick = 2
oplot, x2_blue, h2_blue*100./n2, color = blue, psym = 10, thick = 2
xx1 = mean_region1_DOLP
xx2 = mean_region2_DOLP
yyii = 35
yyjj = 31
xyouts, 2, yyii, 'Means: ', color = black
xyouts, 2, yyjj, 'SDEV (!4r!3)', color = black
xx1 = 4.0
xx2 = 6.0
xyouts, xx1, yyii, string(mean_region1_DOLP, format ="(F5.1)"), color =
red
xyouts, xx1, yyjj, string(sdev_region1_DOLP, format ="(F5.2)"), color =
red
```

```
xyouts, xx2, yyii, string(mean_region2_DOLP, format =“(F5.1)”), color =
blue
xyouts, xx2, yyjj, string(sdev_region2_DOLP, format =“(F5.2)”), color =
blue

; Write DOLP Histogram Plot to File
im = tvrd(true = 1)
write_tiff, Dolp_hist_file + ‘.tif’,   reverse(im,3)
write_jpeg, Dolp_hist_file + ‘.jpg’, im, true = 1, quality = 98

close, 1


      end
```

THIS PAGE INTENTIONALLY LEFT BLANK

LIST OF REFERENCES

Andreou, A. G., & Kalayjian, Z. K. (2002). Polarization imaging: principles and integrated polarimeters. *IEEE Sensors Journal, 2* (6), 566–576.

Coulson, K. L. (1992). Sir David Brewster, Polarization pioneer. *Polarization and Remote Sensing, 1747*, 220–227.

Egan, W. G. (1992). Polarization in remote sensing. *Polarization in Remote Sensing, 1747*, 2–29.

Evans, S. (1965). Dielectric properties of ice and snow–A Review. *Journal of Glaciology*, 773–792.

Eyler, M. (2009). *Polarimetric imaging for the detection of distrubed surfaces.* Naval Postgraduate School, Monterey, CA.

Feynman, R. P. (2006). *The Feynman lectures on physics – definitive edition* (vol. 1). (A. Black, Ed.) San Francisco, CA, USA: Pearson–Addison Wesley.

Haralick, R. M., Shanmugam, K., & Dinstein, I. (1973). Textural features for image classification. *IEEE Transactions on Systems, Man, and Cybernetics, SMC–3* (6), 610–621.

Hecht, E. (2002). *Optics.* Reading, MA: Addison Wesley.

Kuroiwa, D. (1956). The dielectric property of snow. *Union Geodesique et Geophysique Internationale. Association Internationale d'Hydrologie Scientifique*, 52–64.

Lefaudeux, N., Lechocinski, N., Breugnot, S., & Clemenceau, P. (2007). *Compact and robust linear Stokes polarization camera.* Bossa Nova Technologies. Venice: Bossa Nova Technologies.

Olsen, R. C. (2007). *Remote sensing from air and space.* Bellingham, WA: SPIE–The International Society for Optical Engineering.

Pedersen, C. A. (2007). *Optical properties of snow and sea ice – field measurements, parameterization schemes and validation.* University of Tromso, Department of Mathematics and Statistics . Tromso: University of Tromso.

Pedrotti, F. L., & Pedrotti, L. S. (1993). *Introduction to optics* (2nd ed.). Upper Saddle River, NJ: Prentice Hall.

Puetz, A., & Olsen, R. C. (2006). Haralick texture features expanded into the spectral domain. *SPIE, 6233* (623311–1), 12.

Roger, J. C., Santer, R., Herman, M., & Deuze, J. L. (1992). Potentialities in remote sensing of the polarization of the reflected solar light as illustrated from the U.S. space shuttle measurements. *Polarization and Remote Sensing, 1747*, 109–120.

Schott, J. R. (2009). *Fundamentals of polarimetric remote sensing.* Bellingham, WA: Society of Photo–Optical Instrumentation Engineers.

Serway, R. A. (1998). *Principles of physics* (2nd ed., vol. 2). Orlando, FL: Harcourt Brace & Company.

Singh, P., & Singh, V. P. (2001). *Snow and glacier hydrology*. Dordrecht, The Netherlands: Kluwer Academic Publishers.

Smith, P. (2008). *The uses of a polarimetric camera.* Naval Postgraduate School, Monterey: NPS.

Stokes, G. G. (1852). On the composition and resolution of streams of polarized light from different sources. *Cambridge Philosophical Transactions, 9*, 399–416.

Yosida, Z., Oura, H., Kuroiwa, D., Huzioka, T., Kojima, K., & Kinosita, S. (1958). Physical studies of deposited snow. *Applied Physics Section, Institute of Low Temperature Science*, 35.

INITIAL DISTRIBUTION LIST

1. Defense Technical Information Center
   Ft. Belvoir, VA

2. Dudley Knox Library
   Naval Postgraduate School
   Monterey, CA

3. Dr. Richard C. Olsen, Code PH
   Naval Postgraduate School
   Monterey, CA

4. Dr. John R. Schott
   Rochester Institute of Technology
   Rochester, NY

5. Ernie Reith
   Federal Bureau of Investigation
   Washington, D.C.

6. Greg Smith
   National Geospatial-Intelligence Agency
   Ft. Belvoir, VA